PATTERN ANALYSIS AND RECALIBRATION OF A PERFECTLY FORCED ATMOSPHERIC GENERAL CIRCULATION MODEL

by

ANNA GERTRUIDA BARTMAN

Submitted in partial fulfilment

of the requirements for the degree

MASTER OF SCIENCE (METEOROLOGY)

in the

FACULTY OF NATURAL AND AGRICULTURAL SCIENCES

UNIVERSITY OF PRETORIA

PRETORIA

FEBRUARY 2002

"Look, God is exalted beyond

what we can understand.

His years are without number.

He draws up the water vapour

and then distills it into rain.

The rain pours down from the clouds,

and everyone benefits from it."

Job 36:26-28

PATTERN ANALYSIS AND RECALIBRATION OF A PERFECTLY FORCED ATMOSPHERIC GENERAL CIRCULATION MODEL

ANNA G. BARTMAN

Supervisor:	Dr. C.J. de W. Rautenbach
Co-Supervisor:	Dr. W.A. Landman
Department:	Geography, Geoinformatics and Meteorology
University:	University of Pretoria
Degree:	Master of Science (Meteorology)

DISSERTATION ABSTRACT

Empirical techniques are developed to adjust dynamic model forecasts on the seasonal time scale for southern African summer rainfall. The techniques, called perfect prognosis and model output statistics (MOS), are utilized to statistically "recalibrate" general circulation model (GCM) large-scale fields to three equi-probable rainfall categories for December to February. The recalibration is applied to a GCM experiment where simultaneously observed sea-surface temperature (SST) fields serve as the lower boundary forcing, referred to as the simulation mode experiment. Cross-validation sensitivity tests are first performed over a 28-year climate period to design an optimal canonical correlation analysis (CCA) model for each of the two recalibration methods. After considering several potential predictor fields, the 700 hPa geopotential height field is selected as the single predictor field in the two sets of statistical equations that are subsequently used to produce recalibrated rainfall simulations over a 10-year independent test period. Patterns analysis of the predictor and predictand fields suggests that anomalously low (high) 700 hPa geopotential heights over the

subcontinent are associated with wet (dry) conditions over land, an association that is supported by observational evidence of rain (drought) producing systems. Additionally, the dominant mode of the recalibration equations is associated with the El Niño/Southern Oscillation (ENSO) phenomenon. Somewhat higher retro-active skill levels are found using the MOS technique, but the computationally less intensive perfect prognosis technique should also be able to produce usable seasonal rainfall forecasts over southern Africa in an operational forecast environment hampered by the lack of computing resources.

Key words: Pattern analysis; Recalibration; Southern Africa; GCM simulations; Perfect prognosis; Model output statistics; Seasonal rainfall simulations.

PREFACE

Seasonal climate fluctuations have an important influence on society. Rainfall variability has a profound impact on agriculture, food security, water supply and health, particularly in rural communities. In southern Africa, it can make the difference between feast and famine.

The use of skilful climate forecasts can have positive impacts on the quality of life in many areas, of which increased food production in agriculture and water management are amongst the most important. Since the mid-nineties, a progressive number of scientists have entered the climate forecast arena in southern Africa. The ocean-atmosphere interactions responsible for interannual rainfall variability over southern Africa are non-linear and therefore the purely statistical models, which are mostly linear, have made way for more elaborate general circulation models (GCMs) as computer resources have become available. However, climate impacts on the regional scale cannot be accessed directly from GCM output because the spatial resolution of these models is too large for regional scale analysis and also, some output variables are dependent on sub-grid scale processes and can therefore not be simulated reliably. Consequently, downscaling techniques have emerged as a means of relating large-scale GCM output to sub-grid scale variables. Regional analysis can also be done by recalibrating the GCM output by using the same techniques as in downscaling, but the output is not necessarily on a finer grid than that of the GCM. Recalibration of GCM output is often necessary because significant biases occur between the real world and its modelled representation. Systematic biases that typically arise from GCM simulations, for instance spatially distorted patterns of rainfall variability and overestimated rainfall amounts, can be adjusted through recalibration.

The main objective of the research presented in this dissertation is to compare the skill levels of two empirical methods that are used to recalibrate GCM output to summer

rainfall over southern Africa. Here, the GCM is forced with observed sea-surface temperature (SST) anomalies that are simultaneous with the rainfall season in order to use the best estimate of the GCM prognostic fields.

The specific objectives are to:

- ascertain if statistical recalibration of rainfall for southern Africa is possible;
- determine if the chosen predictor fields are physically meaningful; and
- establish which statistical recalibration method gives the higher level of recalibration skill.

These objectives will be pursued through the following steps:

1. construct a 30-year climate through GCM simulations, using the ensemble mean of 5 ensemble members; as well as a 30-year climate record from observed conditions.

2. establish which of the GCM prognostic and observed large-scale fields (to be used as predictor) relate best to rainfall in southern Africa.

3. set up the equations for both recalibration methods.

4. do retro-active simulations of the predictor and recalibration of rainfall over a ten-year independent test period.

5. compare the retro-active skill scores for each recalibration method.

The dissertation consists of five chapters. Chapter 1 describes seasonal forecasts and methods, recalibration, seasonal forecast skill and the geographical area of interest. The rainfall and agricultural profile of South Africa, the relation between sea-surface temperatures and southern African rainfall, as well as the use of seasonal forecasts in

South Africa are discussed. The chapter concludes with the aims of this research. Statistical recalibration techniques are discussed in Chapter 2, with specific reference to perfect prognosis and model output statistics. The following statistical analysis tools are explained: cross-validation, empirical orthogonal functions, canonical correlation analysis, skill measures and forward selection. The CSIRO 9-level atmospheric GCM (CSIRO 9 GCM) is fully described and the data used in this study are noted. In Chapter 3, the statistical model development is described for both methods and the selection of the predictor through forward selection is explained. Pattern analysis is done to establish the physical relationship between the predictor and predictand. The retro-active simulations are covered in Chapter 4. Firstly, the simulation scheme is discussed and the results of the retro-active simulations are shown. The skill scores are calculated, followed by a discussion of specific cases and the conclusion reached through comparison of the results. The summary and conclusions of the study can be found in Chapter 5.

This study forms part of the continuous research conducted at the South African Weather Service (SAWS), specifically aimed at the improving of seasonal forecast products and services to the South African end-user community and neighbouring countries. Some of the results in this dissertation have already been presented at the South African Society for Atmospheric Sciences 2000 conference.

ACKNOWLEDGEMENTS

- The CSIRO 9 GCM was used with the courtesy of the University of Pretoria. I would like to mention Dr. Hannes Rautenbach, who assisted with the setting up of the model and the SST input data.

- The rainfall data used were obtained from the SAWS and the National Meteorological Services of Namibia, Botswana, Lesotho and Swaziland.

- The use of the J90 supercomputer and other computer resources of the SAWS is acknowledged with gratitude. I would also like to mention Mr. Jakkie Barnard who assisted with the archiving of the simulation data

- The much-appreciated help of the SAWS librarians, Mrs. Karin Marais and Elda Stewart, must be mentioned.

- Useful discussions with my colleague, Dr. Emsie Klopper, are gratefully acknowledged.

- I would like to thank Dr. Willem Landman, my supervisor, for his guidance and most valuable contribution to this dissertation.

- Thanks to my husband and parents for their support and encouragement.

CONTENTS

LIST OF FIGURES

LIST OF TABLES

LIST OF ABBREVIATIONS

AGCM	Atmospheric general circulation model
CCA	Canonical correlation analysis
CSIRO	Commonwealth Scientific and Industrial Research Organisation
CSIRO 9 GCM	CSIRO 9-level atmospheric general circulation model
DJF	December-January-February
ENSO	El Niño-Southern Oscillation
EOF	Empirical orthogonal function
GCM	General circulation model
HCM	Hybrid coupled model
LAM	Limited area model
LEPS	Linear Error in Probability Space
LOGIC	Long-term Operational Group Information Centre
MOS	Model output statistics
NCEP	National Centers for Environmental Prediction
R21	Rhomboidal truncation at 21 waves
SAWS	South African Weather Service
SOI	Southern Oscillation Index
SST	Sea-surface temperature

CHAPTER 1

INTRODUCTION

1.1 Background

The variability of climate on seasonal-to-interannual time scale has a profound influence on many facets of human life. The effects of climate variability can be intense, making the difference between wealth and poverty, feast and famine, health and disease, and even life and death. At other times, these effects are more subtle and difficult to separate from other driving forces affecting society, spelling only delicate differences among degrees of profit and loss. Looking to the future, there is enough reason to believe that the welfare of society will increasingly depend on risks and opportunities associated with seasonal-to-interannual climate variability. The global demand for food is rising with the growing population, especially in developing countries where the welfare of the community is mainly dependent on rural farmers.

Increased knowledge of ocean-atmosphere interactions has led to improvement in the ability to forecast climate variability, specifically on the seasonal time scale - one of the foremost advancements in the atmospheric sciences at the close of the 20th century (Stern and Easterling, 1999). Communities can, through the use of improved seasonal climate forecasts, deal with the effects of climate variability more effectively than ever before and use the opportunity to protect, and even to increase, social welfare.

1.2 Seasonal Forecast Models and Methods

Both empirically- and physically-based models are used as methods to forecast seasonal climate variations (Mason *et al.*, 1996). Physical models attempt to forecast the time-average of future atmospheric conditions by simulating the dynamic and

thermodynamic processes which determine the state of the non-linear atmosphere. Empirical models, on the other hand, rely on past statistical associations between atmospheric and oceanic parameters and the climatic variable being forecast (Hastenrath, 1990a, 1990b, 1991; Chu and He 1994).

Statistical forecast techniques have predictive skill that can be ascribed to low frequency changes in the sea-surface temperature (SST) of the oceans, particularly the tropical Pacific Ocean. In some regions and for some variables, statistical models yield better results than physical models (Graham and Barnett, 1995). However, for many regions of the globe, and for many variables, the lack of fundamental data sets (both spatially and temporally) do not permit the construction of statistical specification models. Furthermore, some important climate variables - such as rainfall - are associated with highly nonlinear processes which make them difficult to model statistically (Wilks, 1995). On the other hand, the skill of physical models or atmospheric general circulation models (AGCMs) at long range climate forecasting is virtually nil if they are used without the appropriate SST forcing, because the AGCM by itself lacks knowledge of the ocean memory that the statistical studies have identified as the source of predictive skill. Physical ocean forecast tools by themselves are also of little use for predicting atmospheric changes outside the Pacific equatorial strip (Barnett *et al.*, 1994).

The combination of physical ocean models, AGCMs and statistical models render a more viable approach to seasonal forecasting. Coupled dynamic ocean-atmosphere models are successfully used in the forecasting of climate parameters such as SSTs (Kirtman *et al.*, 1997; Kleeman, 1999; Schneider *et al.*, 1999; Zebiak *et al.*, 1999). When computer resources become a limitation, hybrid coupled models (HCMs) provide a possible solution. Most HCMs use a general circulation model (GCM) to model changes in the ocean, because the ocean accounts for most of the memory of the coupled system and therefore a more accurate representation of the oceanic dynamics is necessary. The fast adjustment of the atmosphere to a changing ocean justifies the use of a steady-state statistical (or empirical) model for the atmosphere. HCMs are a popular forecast tool currently used operationally in long-term forecasting, since they

have been most successful with the simulation of El Niño-Southern Oscillation (ENSO) variability (Barnett *et al.*, 1993; Syu *et al.*, 1995; Pierce, 1996; Blanke *et al.*, 1997). The additional cost and effort involved with a forecast scheme making use of dynamic models can, in general, be justified if it outscores the statistical model used to set a baseline skill (Barnston *et al.*, 1994). It is important that a balance should be attained between improved analysis techniques, enhanced models and the use of ensembles to take optimal advantage of future computing power, which will require changes in both research and operational philosophies (Harrison, 1994).

1.3 Recalibration and Downscaling Techniques

Some of the direct output from GCMs on an inter-annual to intra-annual time scale may be inadequate for assessing seasonal climate impacts on regional scale. Two main reasons exist: Firstly, the spatial resolution of GCMs is too large for smaller scale analysis; and secondly, some output variables (e.g. precipitation) are dependent on sub-grid scale processes (e.g. cloud formation) and can therefore not be simulated reliably (Wilby and Wigley, 2000). Consequently, recalibration techniques have emerged as a means to relate large-scale GCM output to surface variables such as rainfall. Recalibration of GCM output to a horizontal resolution smaller than that of the GCM is generally referred to as downscaling.

There are typically five methods to recalibrate GCM output to regional scale variables (Rummukainen, 1997):

(a) Conventional methods consist of a straight-forward scaling of present-day or climatological local time series with GCM data (e.g., Cubasch *et al.*, 1996). Although this method is easy and cheap to apply, it works mostly through average changes and can not take into account higher-order changes like variances and extreme events. Furthermore, if a GCM performs poorly over a

specific region or time span even on its own grid-scale, conventional methods cannot better the performance.

(b) The main aim of stochastic methods is to overcome the coarse temporal resolution of GCM data through the use of stochastic weather generators (e.g., Wilks, 1989; Racsko *et al.*, 1991; Posch, 1994; Semonov and Barrow, 1997). Weather generators can produce a series of synthetic daily weather data of which the statistical distribution can be dealt with as identical to observations.

(c) Statistical methods will be employed in this study and are discussed in detail in the following chapter.

(d) Dynamical methods extract the local-scale from the large-scale GCM data. This is usually done by one of three approaches: (i) running a limited area model (LAM) on a regional scale with the coarse GCM data as boundary conditions (e.g., Haywood *et al.*, 1997; Charles *et al.*, 1999); (ii) running high-resolution AGCMs with the coarse GCM data as initial conditions (e.g., Pollard and Thompson, 1997; Murphy, 1999, 2000); and (iii) using a variable-resolution GCM with the highest resolution over the area of interest (e.g., Fox-Rabinovitz et al., 1997). While the performances of statistical and stochastic methods are restricted by the link to the observed data, dynamical methods include a physical representation of the climate system. The practical application of this method is, however, limited by the availability of computer resources which is demanded by the increase in resolution.

(e) Composite methods can offer an easy way to construct a number of scenarios and/or combine the results of several GCMs. One method can be used to extract the regional scale, while another is used to arrive at the local scale. The advantage of combining methods is that uncertainties in the climate response and/or emission scenarios can be accommodated.

1.4 Seasonal Forecast Skill

The potential for seasonal predictability is high in the tropics because of the more direct coupling between the atmosphere and the ocean, and the atmospheric internal variability is relatively small in the tropics (Livezey, 1990a, 1990b). In the extratropics, however, greater inherent chaotic instability is found in the atmosphere, especially during the winter, which leads to relatively less potential in seasonal forecasts (Palmer and Anderson, 1994). Forecast skill in the extratropics is regionally and seasonally specific (Buchmann *et al.*, 1990; Zeng, 1990; Palmer and Anderson, 1994), and the highest forecast skill is often found in areas having a strong relationship with the ENSO phenomenon (Mason *et al.*, 1996).

The spatial and temporal variability of seasonal forecast skill over southern Africa is mainly due to the difference in forecastability between the tropical and extratropical atmosphere (Mason *et al.,* 1996), both of which influence the subtropical climate of South Africa (Tyson, 1986; Levey, 1993). Higher skills are found during the peak austral summer months of the summer rainfall region, which are directly related to the predominantly tropical atmospheric circulation influence at this time of year (Mason *et al.,* 1996; Rautenbach and Smith, 2001).

One of the most important influences on the tropical atmospheric circulation over southern Africa are ENSO events (Jury, 1996; Shinoda and Kawamura, 1996; Makarau and Jury, 1997; Mason and Jury, 1997; Rocha and Simmonds, 1997; Mattes and Mason, 1998). The Southern Oscillation Index (SOI) is an indicator of the phase of ENSO (Schulze, 1986), and therefore relatively high forecasts skill levels are found in those areas that are strongly correlated with the SOI (Main and Hewitson, 1995; Mason and Jury, 1997). The correlation between the SOI and the seasonal rainfall over South Africa during October-November-December (early summer) is positive over the greater part of the country, but weak and statistically significant only over limited areas (Lindesay, 1988). During January-February-March (late summer), the strongest

correlation is found over the central parts of South Africa. The same scenario is evident in the analysis of the correlation between NINO3 SSTs and the total rainfall for early and late summer (Kruger, 1999) as depicted in Figure 1.1.

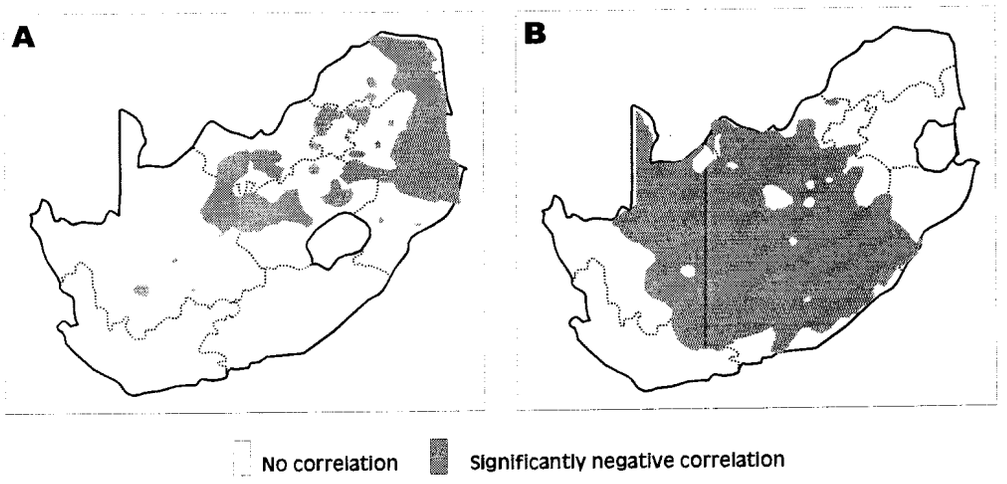

Figure 1.1 The analysis of the correlation between NINO3 SSTs and the total rainfall over South Africa for (a) October-November-December and (b) January-February-March (from Kruger, 1999). The areas of significant negative correlation are shaded.

Another important source of summer rainfall predictability can be found in the northern and central tropical Indian Ocean SSTs (Jury and Pathack, 1991; Mason 1995). A strong correlation with SSTs in these regions contribute to the high forecast skill that is found during January-February, especially in the Northern Province of South Africa (Figure 1.2). However, the linear association between southern African summer rainfall and the equatorial Indian Ocean SSTs may be unstable (Landman and Mason, 1999).

The influence of tropical cyclones over the east-African coast contributes significantly to the inter-annual rainfall variability of the Lowveld (the easternmost part of Mpumalanga - see Figure 1.2), which results in a poor peak summer performance of most seasonal forecast models for this region (Jury 1993; Mason *et al.*, 1996).

Low predictability is found over the western parts of the Western Cape which forms a part of the winter rainfall region of South Africa (Mason and Jury, 1997). The reason for

the low skill can be attributed to the annual influence of extratropical circulation on this part of the country (Mason *et al.*, 1996).

1.5 Rainfall and Vegetation Profile of Southern Africa

South Africa, Lesotho, Swaziland, Namibia and Botswana are included in the southern African region which forms the focal point of this study (Figure 1.2).

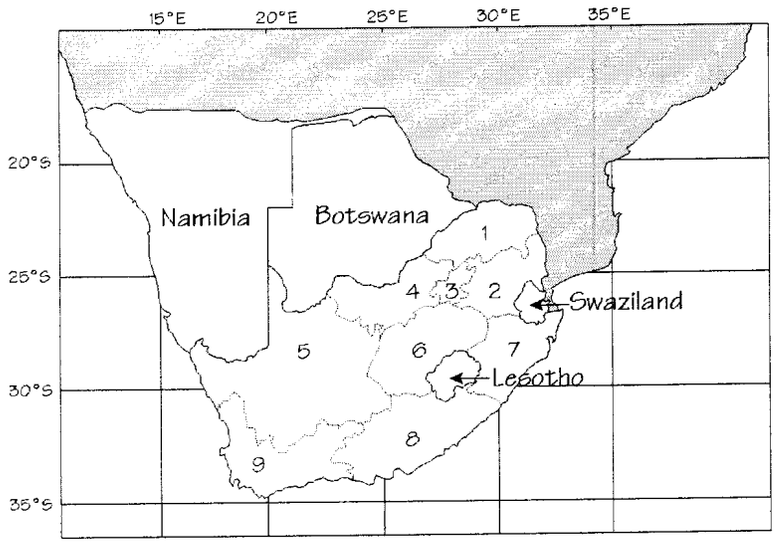

Figure 1.2 The geographical location of southern Africa. Provinces of South Africa: 1 = Northern Province; 2 = Mpumalanga; 3 = Gauteng; 4 = North-West; 5 = Northern Cape; 6 = Free State; 7 = KwaZulu-Natal; 8 = Eastern Cape; 9 = Western Cape.

The rainfall in the southern parts of Africa is highly seasonal. In the larger part of southern Africa, more than 80% of the annual rainfall occurs in the austral summer, between October and March, and is mostly of convective origin (Tyson, 1986). The exception is found in the southwestern parts of the Western Cape province of South Africa where the main rainfall season occurs during the austral winter, i.e. May to August, while the southern coastal regions and adjacent interior receive rainfall throughout the year. The annual rainfall is distributed unevenly across the region, with

dry, arid conditions occurring in the west and humid, subtropical conditions in the east. Figure 1.3 A shows the average annual rainfall for southern Africa, which increase from less than 50 millimetres in the west to more than 900 millimetres in the east.

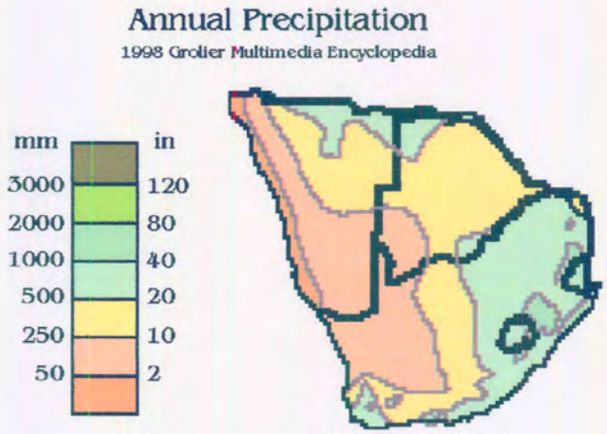

Figure 1.3 A The average annual rainfall distribution (in mm or in) over southern Africa (from Grolier Multimedia Encyclopedia, 1988).

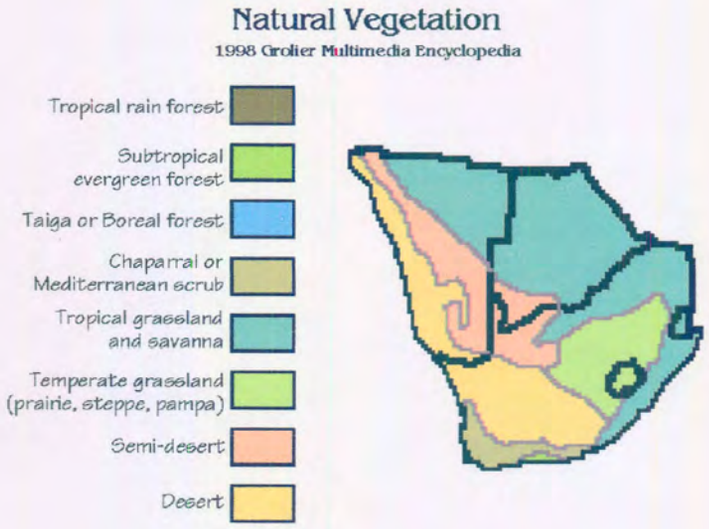

Figure 1.3 B The natural vegetation of southern Africa (from Grolier Multimedia Encyclopedia, 1988).

The natural vegetation of southern Africa (Figure 1.3 B) ranges from desert-like vegetation in the west to grassland and savanna in the northern and eastern parts. Mediterranean scrub are found in the winter rainfall regions of South Africa.

1.6 Sea-Surface Temperatures and Southern African Rainfall

It is well-known from empirical studies that there is a close, simultaneous relationship between changes in tropical SST and various atmospheric variables over many regions of the world (Barnett *et al.*, 1994). For example, SSTs in different ocean regions have a combined effect on seasonal rainfall in southern Africa (Mason *et al.*, 1996; Jury *et al.*, 1999; Landman and Mason, 1999). The ENSO phenomenon, which involves changes in SSTs in the equatorial Pacific Ocean, has a profound influence on rainfall over most parts of southern Africa (Ropelewski and Halpert, 1987, 1989; Main and Hewitson, 1995; Shinoda and Kawamura, 1996; Mason and Jury, 1997; Rocha and Simmonds, 1997; Mattes and Mason, 1998). Figure 1.4 depicts "core regions" of consistent ENSO-related precipitation for equatorial and southern Africa. Rainfall in the summer rainfall regions of South Africa tends to be anomalously low (high) during El Niño (La Niña) events when SSTs in the equatorial Pacific Ocean are anomalously high (low).

SSTs in the oceans surrounding southern Africa also play an important role in rainfall variability over the subcontinent (Nicholson and Entekhabi, 1987; Walker, 1990; Jury and Pathack, 1991; Mason, 1995; Mason and Jury, 1997; Rocha and Simmonds, 1997; Reason and Lutjeharms, 1998; Landman and Mason, 1999; Reason, 1999). The ENSO signal in Indian Ocean SSTs has weakened since the late 1970s, changing the relationship between SSTs in the Indian Ocean and summer rainfall over southern Africa: over the most recent two decades, warm (cold) events in the tropical western Indian Ocean have become, to a higher degree, associated with wet (dry) conditions over the north-eastern half of southern Africa (Landman and Mason, 1999). It is therefore necessary that the effects of global ocean anomalies on southern African rainfall are taken into account when producing seasonal forecasts for this area.

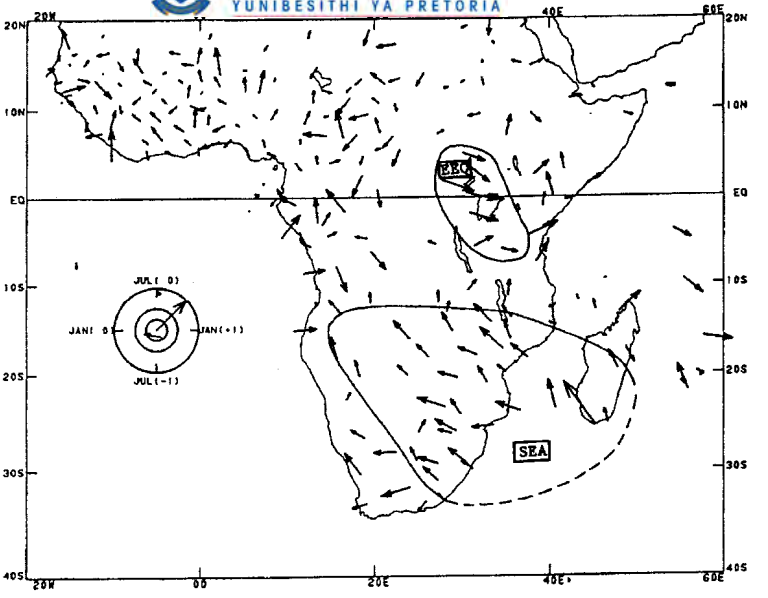

Figure 1.4 Subjectively determined "core regions" of consistent ENSO-related precipitation for equatorial and southern Africa. Areas where the boundaries are not well defined are indicated by dashed lines. (Ropelewski and Halpert, 1987)

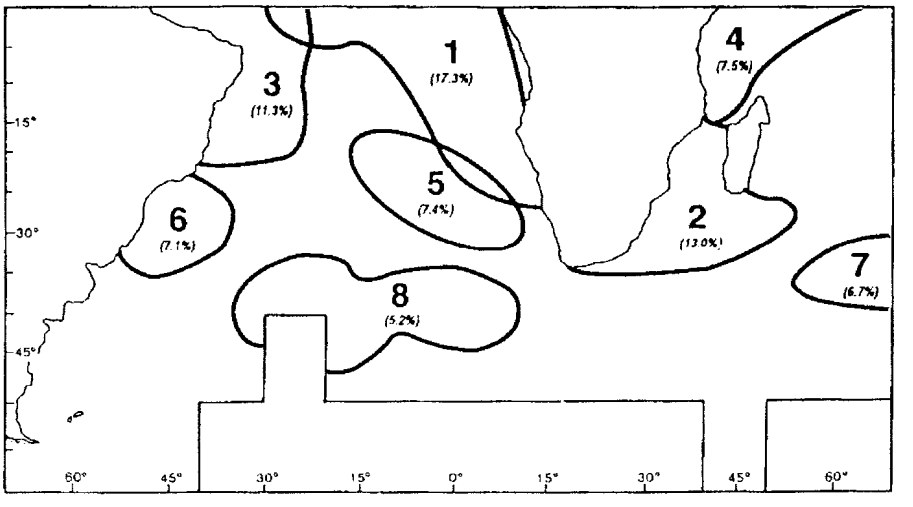

Figure 1.5 Core areas of SST coherence (Mason, 1995).

Figure 1.5 shows the significant areas in the oceans adjacent to southern Africa (Mason, 1995). SSTs off the east coast (region 2) seem to have a significant influence on

systems governing the rainfall over the subcontinent by enhancing both tropical and temperate synoptic systems which affect rainfall throughout most of the year. Anomalous convection over the western equatorial Atlantic Ocean (region 3) may have an effect on westerly waves, while SST anomalies over the western tropical Indian Ocean (region 4) influence the easterly tropical disturbances.

1.7 The use of Seasonal Forecasts in South Africa

One of the most important elements for planning future activities in modern societies in an intelligent manner is the ability to forecast climate variations skilfully (Moura, 1994). Skilful climate forecasts can most certainly have positive impacts on the quality of life in many areas: increased food production in agriculture (seed selection and allocation) and fisheries, forest management and river control (water restriction plan, flood control), as well as hydroelectric power generation and distribution. It is important to note that the benefits of climate forecasts are strongly related to the user's will to apply the information available. A climate forecast can be considered useful if the forecast has skill, the parameters are relevant to the user and the forecast is timely in relation to actions the user can take to improve outcomes (Stern and Easterling, 1999).

South Africa covers an area of 122.3 million hectares, of which 84% is used for agricultural purposes. A large part of the arable area is used for pasture, but maize, wheat and sugar cane form the basis of the major consumer products cultivated (National Department of Agriculture, 1997). The most important factor limiting agricultural production is the availability of water (Klopper and Bartman, 2001). Nearly half of South Africa's available water is used for agricultural purposes, while hydroelectric power generation, industries and domestic use also claim a share. Careful planning of water usage is therefore inevitable and seasonal forecasts are of utmost importance in this process, not only for water management purposes, but also for subsistence and commercial farmers.

In order to produce accurate and socio-economically relevant climate information and to disseminate the forecast products timely it is necessary to follow a well-established strategy. Different research groups in South Africa are involved in the research of suitable seasonal forecast methods (Mason *et al.*, 1996), but most of them do not have the resources to build and maintain relationships with end-users. It is of utmost importance to tend to the users' needs and the problems they encounter with the application of climate forecast information. The Long-term Operational Group Information Centre (LOGIC)[1] was established in October 1996 at the South African Weather Service (SAWS) to overcome this gap between the producers and users of seasonal forecasts in South Africa. Several models from different national and international institutions are used to compile a single consolidated seasonal outlook for southern Africa each month. These models comply to certain evaluation standards and outscore baseline skill levels set by statistical models used with success at the SAWS (Klopper and Landman, 2002). The LOGIC does not only disseminate this outlook to end-users in various sectors ranging from agriculture and farming to disaster management and planning (Table 1.1), but also a wide variety of real-time information. These services rendered by the LOGIC has been found to be very useful and extremely relevant: The results of a survey done after the 1997/98 El Niño season show (i) that farmers and other end-users took definite action in response to the seasonal outlook; and (ii) 80% of the respondents stated that they had been better off having the information on expected rainfall and temperature conditions available (Klopper, 1999). These results were echoed by surveys done after the 1998/99 and 1999/2000 summer rainfall seasons (Klopper and Bartman, 2001).

[1] http://www.weathersa.co.za/nwp/m2ltproducts.html

Table 1.1 The field of speciality of individuals who responded to questionnaires after the 1997/98, 1998/99 and 1999/2000 austral summer rainfall seasons. (From Klopper, 1999).

Sector	Speciality
Climatology / Meteorology	Research
Energy	Dehumification of substation Energy supply
Water	Water management Agrohydrology
Food Industry	Food analysis Food processing
Farming (Commercial and Small farmer)	Citrus, Sugar, Forestry, Cut flowers, Maize, Wheat, Vegetables, Pasture seed, Tobacco, Sunflower, Cotton, Grazing, Soya bean, Tea, Coffee, Cash crops, Fruit, Dry beans, Sugar cane, Stock (sheep, cattle, milk), Wildlife, Ostrich
Nature conservation	Nature conservation
Construction	Dam construction, Roof repairing
Policy-making	Government policy for agriculture Disaster management Strategic planning Food security
Education	Training

1.8 Hypothesis

The use of GCMs in the seasonal forecasting arena has become essential, since the ocean-atmosphere interactions responsible for the interannual rainfall variability over southern Africa are non-linear and cannot be taken into account by statistical models

which are mostly linear. Furthermore, the association between southern Africa's summer rainfall and SSTs in the equatorial Indian Ocean is unstable, which adversely affects statistical models (Landman and Mason, 1999).

Until the recent past, mostly statistical models had been used in seasonal forecasts for South Africa. Model output from GCMs run at international institutions are available, but usually on a global coarse grid-scale. A multi-tiered forecast scheme had been developed by Landman *et al.* (2001a), using statistical near-global SST forecasts (Landman and Mason, 2001) to force the COLA T30 GCM (Kirtman *et al.*, 1997). The large-scale GCM simulations of circulation and moisture at certain levels were then *recalibrated* to produce rainfall forecasts successfully at the regional level using the perfect prognosis approach (Wilks, 1995).

This study has been framed within the hypothesis that recalibrated GCM output can be used successfully to provide operational seasonal rainfall forecasts for southern Africa and that they have the potential to outscore simple statistical models. The main objective of this study is to compare two statistical recalibration methods: the first method uses a GCM simulated climate record, while the second method makes use of an observed climate record (Wilks, 1995). The first approach, being a more elaborate method, takes the systematic errors of the GCM into account, but uses more computer resources than the second method. If the two methods produce about equally skilful simulations, the method using an observed climate which requires much less computer resources, could be used instead. The specific objectives, method and organisation of this dissertation are explained in the Preface.

CHAPTER 2

METHODS AND DATA

2.1 Introduction

Statistical recalibration methods use long-term time series to construct statistical relationships between small-scale variables and large-scale features of surface or atmospheric parameters. Two methods of statistical recalibration are compared in this study, using firstly large-scale parameters simulated by a GCM, and secondly observed atmospheric parameters, to derive austral summer rainfall quantities over southern Africa.

2.2 Statistical recalibration methods

2.2.1 Perfect Prognosis

The perfect prognosis technique assumes the GCM forecasts of future atmospheric variables to be perfect, making no attempt to correct for possible GCM errors or biases (Wilks, 1995). Regression equations for this technique are developed by using the observed predictors to specify observed predictands. That is, only historical climatological data are used in the development of a perfect prognosis forecast equation. Furthermore, these equations do not incorporate any time lag, but simultaneous values of predictors and predictands are used to fit the regression equations. The forecast time lag in the perfect prognosis approach is contained entirely in the GCM, because the GCM forecasts of the predictors are substituted into the regression equation as predictor values. The performance of this technique is therefore dependent on the GCM: If the GCM forecasts were perfect, the perfect prognosis

regression equations would provide very skilful forecasts, provided that a strong statistical relationship exists between the predictor and predictand variables. In perfect prognosis, no attempt is made to compensate for the systematic errors present in the GCM. However, bias corrections can be applied to the GCM data before it is used in the perfect prognosis equations (Landman *et al.*, 2001b).

2.2.2 Model Output Statistics

The MOS approach (Glahn and Lowry, 1972) includes the influences of specific characteristics of the GCM directly in the regression equation, therefore it is a usually preferred method for recalibration. The MOS approach uses GCM predictors in both the development of the statistical equations and the implementation thereof, while perfect prognosis uses the GCM predictors only when making forecasts. In setting up the MOS equations it is therefore necessary to have GCM-produced fields for an extended time period to construct the climate of the predictors. Unlike perfect prognosis, the implementation of a MOS forecast equation is consistent with its development, giving rise to the fact that separate MOS equations must be developed for different forecast projections and for different GCMs, which makes the use of a MOS recalibration approach only feasible if a substantial amount of computer resources are available (Wilks, 1995).

2.3 Statistical Analysis Tools

2.3.1 Cross-validation

The method of cross-validation (Barnett and Preisendorfer, 1987; Michaelsen, 1987; Barnston and van den Dool, 1993) can be used to establish the regression equations' performance. One year is omitted from the predictor and predictand training period, and the model is trained using the remaining year's data. The one-year-out cross-validation design is adequate here because all of the regions are associated with one-year and

longer lag autocorrelation values that are associated with statistical significance less or equal to the 90% level of confidence. The model simulation is then tested against the predictand which was withheld from the training period. This procedure is repeated for all the years in the training period to produce a set of simulations. The simulated years are then compared with the observed set to estimate the scheme's performance.

2.3.2 Empirical Orthogonal Function

Pre-orthogonalization (Barnston, 1994) on the predictor fields, and to a lesser extend on the predictand fields, is necessitated by the large number of highly correlated variables and few observations. A standard empirical orthogonal function (EOF) analysis (Preisendorfer, 1988; Jackson, 1991; von Storch and Navarra, 1995) is employed for this purpose. The variances of the parameters used as possible predictor variables differ and therefore standardization is done. Standardising the data sets also ensures that all the elements have equal opportunity to participate in the prediction process (Jackson, 1991; Barnston, 1994). EOF analysis is performed separately for each of the predictor and predictand sets, retaining only those modes that are physically meaningful.

2.3.3 Canonical Correlation Analysis

Both the MOS and perfect prognosis recalibration schemes incorporate the use of a statistical method to relate the large-scale predictor fields to regional rainfall indices. Canonical correlation analysis or CCA (Barnett and Preisendorfer, 1987; Graham et al., 1987a, 1987b; Tatsuoka, 1988; Jackson, 1991; Barnston and Ropelewski, 1992; Barnston, 1994; Chu and He, 1994; Barnston and Smith, 1996) is used as the statistical tool in the recalibration. CCA is a multi-variate statistical method used to determine the linear combination between a predictor and predictand data set.

Consider two vectors: **X** as predictor and **Y** as predictand, where the number of spacial

elements in the predictand set is smaller than that of the predictor. CCA finds the canonical vectors (**u**,**v**) and linear combinations of **Z** = **u**'**X** and **W** = **v**'**Y**, such that the canonical variates **Z** and **W** are optimally correlated. The prime in the equations denotes the transpose of the vectors. Once the first pair of linear combinations has been found, the following pair of linear combinations that are most strongly correlated is identified. This new pair must be orthogonal to the previously found pair(s). A variety of methods exist to aid in the selection of significant CCA modes. The Guttman-Kaiser approach (Jackson, 1991) is used during the analysis to select the number of CCA modes to be retained. This approach discards any eigenvalues smaller than the mean of the eigenvalues.

2.3.4 Skill measures

Hit scores (Wilks, 1995), as well as the Linear Error in Probability Space (LEPS) score (Ward and Folland, 1991; Potts *et al.*, 1996) are used as skill estimates to establish the model's performance over ten retro-active simulation years.

2.3.5 Forward selection

Forward selection is the most commonly used form of screening regression (Wilks, 1995). The process can be described as follows: Consider three parameters A, B and C. Each of them is used separately as potential predictor in a cross-validation procedure and the cross-validation correlation for each case is determined. If B yields the highest correlation, it is used in combination with A and C for the next stage of the forward selection, i.e. BA and BC are used as predictors, where BA consists of the combined B and A predictor fields and BC of the combined B and C fields. If BC yields the highest correlation, then BCA will be used as predictor in the final round. Although the specific combination of predictors is important, their order is not. Therefore, BCA will yield the same results as ABC or CBA. In this study the cross-validation correlation, averaged over the summer rainfall regions, is used to determine the importance of the potential predictors.

2.4 The CSIRO 9-level Atmospheric General Circulation Model

2.4.1 GCM characteristics

The AGCM used in this study is a spectral 9-level AGCM, developed at the Commonwealth Scientific and Industrial Research Organisation (CSIRO) Division of Atmospheric Research and is referred to as the CSIRO 9 GCM (McGregor *et al.*, 1993). The model was originally intended to provide the basis for a greenhouse research project and for further research in the multi-season forecast regime at CSIRO, but it is believed that the applicability of the CSIRO 9 GCM in seasonal rainfall forecasting over southern Africa can be justified, a notion that will be tested here.

The version of the CSIRO 9 GCM used here has self-determining lower boundary conditions. The boundary conditions over land are generated by a heat balance requirement at the surface, while those over the oceans are calculated from the use of implied oceanic heat transports. The lower boundary condition for the atmosphere is determined by an interactive land surface scheme but SSTs are prescribed in the model version described here. Sea-ice is also computed, and the polar ice sheets are effectively defined by their surface albedo. The CSIRO 9 GCM performs a forward-in-time integration of the primitive equations describing the motion of the global atmosphere. The model simulates a comprehensive range of "physical" processes including radiation and precipitation which act as forcings of the dynamical equations. Since the model was originally intended for general climate simulation, it represents full annual and diurnal cycles. All other major properties such as cloud amount, snow, and sea-ice are self-determining. Details of the model dynamical equations are given by Gordon (1981), Mc Gregor *et al.* (1993) and Rautenbach (1999).

The model is run at a spectral resolution of R21 (rhomboidal truncation at 21 waves) which gives rise to an equally spaced east-west grid of 64 points and a Gaussian pole to equator grid of 28 unevenly spaced latitudes per hemisphere. A semi-implicit

leapfrog time scheme is used (i.e. current and previous time step values are retained) together with a Robert (Asselin) time filter. The R21 model time step is 30 minutes.

The model utilizes the sigma coordinate system in the vertical, where sigma is the relationship between the pressure on the given level and the surface pressure. Therefore, the vertical level spacing does not need to be uniform. The model integrates the primitive equations over nine full-levels in the atmosphere as shown in Figure 2.1.

AGCMs have demonstrated skill in the reproduction of observed conditions when forced by prescribed observed SSTs (Livezey *et al.*, 1996; Smith and Livezey, 1999, Rautenbach and Smith, 2001). Therefore, in order to use the best estimate of the GCM prognostic fields in the recalibration equations, observed SSTs are used as input data for the CSIRO 9 GCM. The SST data (Smith *et al.*, 1996) were reconstructed to fit the CSIRO 9 GCM grid scale. The model grid scale, shown in Figure 2.2, consists of a total of 56 longitudinal rows and 64 latitudinal columns.

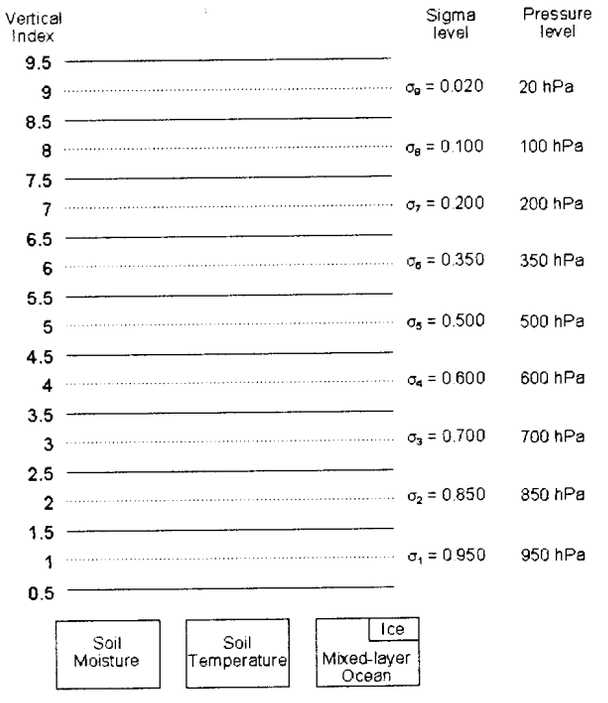

Figure 2.1 Simplified vertical level structure of the CSIRO 9 GCM (after McGregor *et al.*, 1993).

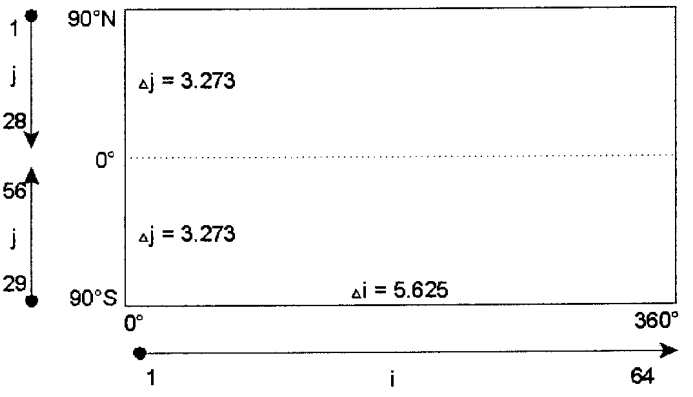

Figure 2.2 The CSIRO 9 GCM horizontal grid scale

The CSIRO 9 GCM is used to simulate geopotential height and moisture data at the pressure levels specified in Figure 2.1, as well as sea-level pressure and rainfall data. The archived geopotential height data at 850, 700, 500 and 200 hPa, as well as the moisture data at 700 hPa, are used in the construction of the recalibration equations.

2.4.2 GCM simulations

The inter-annual variability of the atmosphere at middle- and high latitudes is strongly dominated by internal random variability, which necessitates an ensemble approach (Bengtsson *et al.*, 1996). A number of suggestions to initialize GCM runs currently exists (Hunt, 1997), which includes, amongst others: optimally growing unstable modes in atmospheric initial conditions produce an initial perturbed ensemble (Palmer *et al.*, 1990); the breeding of growing modes (Toth and Kalnay, 1993); and perturbations to the physical parameterization of the model (Harrison, 1994).

The use of different model restart conditions (Barnett, 1995) is employed to initialize ensemble members in this study. The first initial field consists of the output result from a 50-year seasonal cycle run performed with a fixed SST climate. From here the model is forced with observed SST fields starting from January 1968 to December 1997. A

continuous seasonal cycle run is performed over this period, using the result from the end of the previous year to serve as an initial field for the following year. To allow the model to adjust to the newly forced SST patterns, the first simulation year, 1968, is used for model spin-up, followed by the 29-year period of GCM simulations from January 1969 to December 1997. The climate control run for the first ensemble member is used as start-up file for the second, and so forth. As a final result, 5 ensemble members for each month over a period of 29 years forced with observed SST fields have been produced. These GCM fields are referred to as simulation mode fields.

Theoretically, the number of ensemble members used will depend upon the internal variability of the specific GCM used (Kumar and Hoerling, 1995; Barnett *et al.*, 1994). The effective number has a latitudinal dependence. In the tropics, a three- to five-member ensemble appears adequate for a stable forecast (Barnett *et al.*, 1994; Harrison, 1994; Bengtsson *et al.*, 1996), while a six- to ten-member ensemble is preferred for the extra-tropics (Kumar and Hoerling, 1995; Barnett *et al.*, 1994; Moura, 1994). In practice, however, the number of ensemble members that can be run is greatly affected by available computer resources. For the purpose of this study, it was decided to use a five-member ensemble, as has been successfully employed by Bengtsson *et al.* (1996) in simulating the global atmospheric response to the SST forcing, as well as by Rautenbach and Smith (2001).

2.5 Data

2.5.1 Predictor variables

There is little consensus amongst authors as to the choice of atmospheric parameters to be used as predictors in statistical recalibration (Wilby and Wigley, 2000). A wide variety of recalibration predictors has been employed in recent studies when recalibrating GCM output to precipitation. Although there is a tendency to use

circulation parameters as predictors, other variables have been used with success, for example: wind direction and cloud cover (Hay *et al.,* 1992); monthly precipitation (Wilks, 1992); thermodynamic parameters (Perica and Foufoula-Georgiou, 1996); and teleconnection indices (Woodhouse, 1997). The interpretive power of any given predictor varies both spatially and temporally (Huth, 1999). Atmospheric circulation and moisture fields have been found to be important in the recalibration of GCM output to seasonal rainfall over southern Africa (Landman *et al.*, 2001b). In this research, the geopotential heights of the 850, 700, 500 and 200 hPa pressure levels, as well as the moisture at the 700 hPa level, are considered as potential predictors in the equations relating the GCM large-scale to regional DJF rainfall over southern Africa.

2.5.2 NCEP Reanalysis Data

The NCEP reanalysis data (Kalnay *et al.*, 1996) are used as predictor set in the development of the perfect prognosis equations. Monthly averages of geopotential height at the 850 hPa, 700 hPa, 500 hPa and 200 hPa levels are obtained, as well as the moisture at 700 hPa. Seasonal averages for December-January-February (DJF) are calculated for each parameter for the period 1969/70 to 1996/97.

2.5.3 Rainfall data

Nine homogeneous rainfall regions were defined over southern Africa (Mason, 1998; Landman *et al.*, 2001a) from monthly station data covering South Africa, Namibia, Botswana and Lesotho. Rainfall indices were calculated for the period 1950 to 1997 for each of these regions. The regions, as illustrated in Figure 2.3, are the two winter rainfall regions: south-western Cape and south coast; and the summer rainfall regions: Transkei, KwaZulu-Natal coast, Lowveld, north-eastern Highveld, central interior, western interior, and northern Namibia/western Botswana. It was decided to use the target season DJF, since this is an important three-month period for agricultural activities in the summer rainfall region of South Africa. The indices for DJF 1950/51 to 1996/97 are used as the predictand data set.

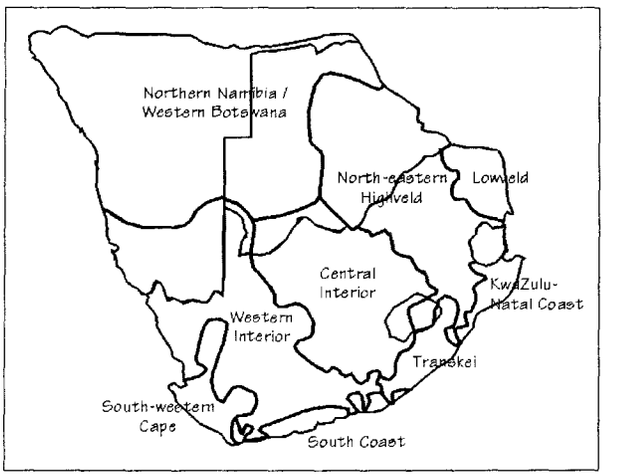

Figure 2.3 The nine homogeneous rainfall regions over southern Africa.

2.6 Summary

The recalibration methods, MOS and perfect prognosis, to be used in this dissertation to relate large-scale atmospheric parameters to southern Africa summer rainfall, have been presented. Both the AGCM (CSIRO 9 GCM) and the statistical model (CCA) have been discussed in some detail, together with the data sets used to set up the recalibration equations. The process of setting up these equations will subsequently be discussed in the next chapter.

CHAPTER 3

THE RECALIBRATION MODELS

3.1 Statistical Model Development

Since GCM simulations are subject to error, statistical recalibration based on the GCM information can improve on aspects of GCM forecasts. The CSIRO simulated rainfall for October to March is compared to the observed rainfall for the corresponding season. The CSIRO 9 GCM simulated a north-south gradient (Figure 3.0A), while the observed rainfall map (Figure 3.0B) shows an east-west gradient. The rainfall amount is also not captured by the GCM simulation. Because of this spatial bias, the necessity for recalibration is evident.

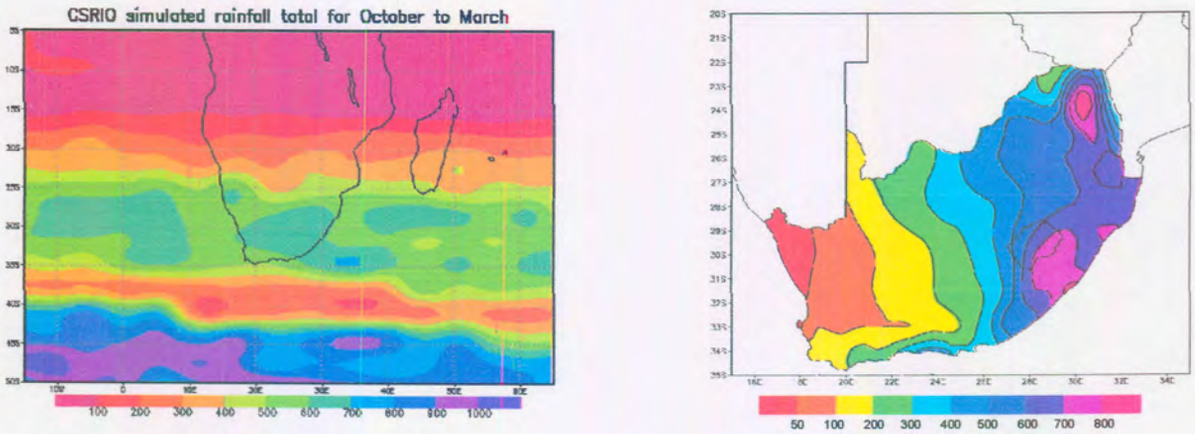

Figure 3.0 The total rainfall (mm) distribution during the main summer rainfall months (October to March) for (a) the CSIRO 9 GCM simulations over southern Africa and (b) observed data over South Africa (from SAWS).

Statistical recalibration is based on the following assumptions: (i) Relationships exist between larger grid scale and surface variables such as rainfall; (ii) these empirical relationships are valid under future climate conditions; and (iii) the larger grid scale

variables and their changes are well characterized by GCMs (Wilby and Wigley, 2000). Simple or extensive statistical methods can be used, but the final relationship between the simulated large-scale and a forecast quantity is usually the result of some form of regression analysis. Here, two approaches are considered to compile the regression equations, namely perfect prognosis and model output statistics (MOS).

The statistical models for both MOS and perfect prognosis are set up over a climate period of several decades. Various parameters are used to investigate possible predictors, namely the geopotential heights at 850, 700, 500 and 200 hPa, as well as 700 hPa moisture. These parameters were previously used to successfully relate large-scale parameters to DJF rainfall over southern Africa (Landman *et al.*, 2001a). For perfect prognosis, the NCEP reanalysis data are used as climatology, while the CSIRO 9 GCM simulations are averaged over 5 ensemble members to establish the climate data for MOS. A window is extracted from both the GCM (Figure 3.1A) and NCEP (Figure 3.1B) data to cover the area of interest (Figure 2.3), i.e., the homogeneous rainfall regions of southern Africa and the subcontinent's adjacent oceans. Only the DJF season is considered in the analysis, since tropical atmospheric circulation becomes dominant during these peak austral summer rainfall months and a higher forecast skill is consequently possible (Mason *et al.*, 1996). The average for each of the parameters is calculated for DJF. Rainfall indices for the period DJF 1969/70 to 1996/97 over the summer rainfall regions are used as the predictand data set.

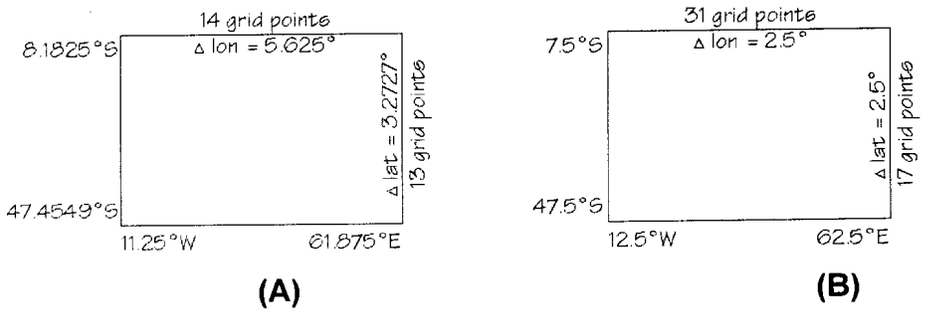

Figure 3.1 The extracted window for (A) the CSIRO 9 GCM simulations and (B) the NCEP reanalysis data.

EOF analysis is performed on the predictor and predictand fields and modes of variability representing physical features, for example ENSO, are produced. Cross-validation is used to determine the optimal number of EOF modes to be retained in the CCA eigen analysis problem. A varying number of predictor (Lx) and predictand (Ly) modes are used, with Lx greater or equal to Ly. The cross-validation correlation is considered for each case, averaged over the summer rainfall regions. Using the maximum cross-validation correlation, the optimum numbers of modes found for MOS are two predictand and two predictor modes, and for perfect prognosis two and three respectively. The explained variance of the predictand is 83.4%, while that of the predictor is 75.1% for MOS and 79.9% for perfect prognosis. CCA is then performed and two modes are selected, using the Kaiser-Guttman criterion (Jackson, 1991).

3.2 Selecting the Predictors

The selection of the predictor fields to be used in the CCA equations is based on a forward selection scheme (Wilks, 1995). Only those fields or combination of fields that provide the highest average cross-validation correlation over the summer rainfall regions are considered. The candidate predictor fields are the 850, 700, 500 and 200 hPa geopotential height fields, as well as the 700 hPa moisture field. The cross-validation correlations for varying numbers of predictor and predictand modes, averaged over the summer rainfall regions, for MOS and perfect prognosis are listed separately in Tables 3.1 to 3.10.

3.2.1 Perfect Prognosis

The highest correlation is found when the geopotential heights at 700 hPa are used as predictor in the perfect prognosis equations (Table 3.1), although the same correlation value of 0.71 is obtained when the geopotential height at 500 hPa field is combined with the 700 hPa geopotential height field (Table 3.2). The geopotential height at 850 hPa, combined with the geopotential heights at 700 and 500 hPa, also produced a cross-

validation correlation of 0.71 (Table 3.3). As a result, the outcome of the forward selection procedure for perfect prognosis points to one of the following combinations: (i) geopotential height at 700 hPa; (ii) geopotential height at 500 hPa combined with (i); or (iii) geopotential height at 850 hPa combined with (ii).

The differences in the average cross-validation correlations associated with each of the reanalysis fields, or combination of fields, are very small in most cases. By comparing the time scores of the first EOF mode of the 700 hPa geopotential height field with those of the other candidate fields or combination of fields that produced the next best average correlation values, significant agreement is found (correlations > 0.9). This agreement indicates that there would be very little difference in skill of the recalibrated simulations using the other fields or combination of fields as predictors instead of only the 700 hPa geopotential heights. Therefore, the inclusion of these former fields is redundant in setting up the optimal perfect prognosis equations.

3.2.2 Model Output Statistics

The highest average cross-validation correlation for MOS is associated with the combined fields of the 700 hPa geopotential heights and moisture (Table 3.7). However, the average correlation of the combined fields is only marginally larger than that of the 700 hPa geopotential heights used on its own in the MOS equations (Table 3.6). In addition, there is, as with the perfect prognosis, a very high association between the EOF mode 1 time scores of the combined 700 hPa moisture and geopotential height fields and the 700 hPa field.

Table 3.1 The cross-validation correlations, averaged over the summer rainfall regions, for varying numbers of predictor and predictand modes, for single predictor variables used in the perfect prognosis equations. The highest mean correlation values are shaded, and values indicated with an asterisk are significant at the 95% confidence level.

Geopotential height at 200 hPa						
Number of modes		Predictor				
		2	3	4	5	6
Predictand	2	0.35	0.50*	0.57*	0.54*	0.59*
	3	-	0.50*	0.57*	0.54*	0.59*
	4	-	-	0.57*	0.55*	0.58*

Geopotential height at 500 hPa						
Number of modes		Predictor				
		2	3	4	5	6
Predictand	2	0.51*	0.59*	0.57*	0.63*	0.68*
	3	-	0.59*	0.57*	0.63*	0.69*
	4	-	-	0.56*	0.63*	0.68*

Geopotential height at 700 hPa						
Number of modes		Predictor				
		2	3	4	5	6
Predictand	2	0.57*	0.61*	0.60*	0.58*	0.70*
	3	-	0.62*	0.60*	0.58*	0.71*
	4	-	-	0.59*	0.58*	0.71*

Geopotential height at 850 hPa						
Number of modes		Predictor				
		2	3	4	5	6
Predictand	2	0.52*	0.60*	0.60*	0.59*	0.63*
	3	-	0.60*	0.60*	0.59*	0.64*
	4	-	-	0.59*	0.59*	0.63*

Humidity at 700 hPa						
Number of modes		Predictor				
		2	3	4	5	6
Predictand	2	0.53*	0.55*	0.52*	0.51*	0.52*
	3	-	0.55*	0.53*	0.52*	0.53*
	4	-	-	0.50*	0.49*	0.50*

Table 3.2 As in Table 3.1, but for two combined predictor variables.

Geopotential height at 700 hPa with Geopotential height at 200 hPa						
Number of modes		Predictor				
		2	3	4	5	6
Predictand	2	0.47*	0.63*	0.59*	0.67*	0.65*
	3	-	0.63*	0.59*	0.67*	0.65*
	4	-	-	0.59*	0.67*	0.65*

Geopotential height at 700 hPa with Geopotential height at 500 hPa						
Number of modes		Predictor				
		2	3	4	5	6
Predictand	2	0.54*	0.61*	0.59*	0.62*	0.70*
	3	-	0.61*	0.59*	0.63*	0.71*
	4	-	-	0.58*	0.62*	0.71*

Geopotential height at 700 hPa with Geopotential height at 850 hPa						
Number of modes		Predictor				
		2	3	4	5	6
Predictand	2	0.55*	0.61*	0.60*	0.59*	0.68*
	3	-	0.61*	0.61*	0.59*	0.69*
	4	-	-	0.59*	0.59*	0.70*

Geopotential height at 700 hPa with Humidity at 700 hPa						
Number of modes		Predictor				
		2	3	4	5	6
Predictand	2	0.60*	0.67*	0.67*	0.64*	0.64*
	3	-	0.67*	0.66*	0.64*	0.64*
	4	-	-	0.65*	0.63*	0.63*

Table 3.3 As in Table 3.1, but for three combined predictor variables.

Geopotential height at 700 hPa and Geopotential height at 500 hPa with Geopotential height at 200 hPa						
Number of modes		Predictor				
		2	3	4	5	6
Predictand	2	0.49*	0.61*	0.57*	0.66*	0.67*
	3	-	0.61*	0.57*	0.66*	0.67*
	4	-	-	0.57*	0.67*	0.67*

Geopotential height at 700 hPa and Geopotential height at 500 hPa with Geopotential height at 850 hPa						
Number of modes		Predictor				
		2	3	4	5	6
Predictand	2	0.54*	0.61*	0.60*	0.61*	0.69*
	3	-	0.61*	0.60*	0.61*	0.71*
	4	-	-	0.59*	0.61*	0.71*

Geopotential height at 700 hPa and Geopotential height at 500 hPa with Humidity at 700 hPa						
Number of modes		Predictor				
		2	3	4	5	6
Predictand	2	0.56*	0.65*	0.64*	0.64*	0.63*
	3	-	0.65*	0.64*	0.64*	0.63*
	4	-	-	0.64*	0.64*	0.62*

Table 3.4 As in Table 3.1, but for four combined predictor variables.

Geopotential height at 700 hPa, Geopotential height at 500 hPa and Geopotential height at 850 hPa with Geopotential height at 200 hPa						
Number of modes		Predictor				
		2	3	4	5	6
Predictand	2	0.50*	0.61*	0.58*	0.68*	0.67*
	3	-	0.61*	0.58*	0.68*	0.68*
	4	-	-	0.58*	0.68*	0.67*

Geopotential height at 700 hPa, Geopotential height at 500 hPa and Geopotential height at 850 hPa with Humidity at 700 hPa						
Number of modes		Predictor				
		2	3	4	5	6
Predictand	2	0.55*	0.65*	0.63*	0.64*	0.65*
	3	-	0.65*	0.63*	0.64*	0.66*
	4	-	-	0.62*	0.63*	0.65*

Table 3.5 As in Table 3.1, but for all five combined predictor variables.

Geopotential height at 700 hPa, Geopotential height at 500 hPa, Geopotential height at 850 hPa and Geopotential height at 200 hPa with Humidity at 700 hPa						
Number of modes		Predictor				
		2	3	4	5	6
Predictand	2	0.52*	0.64*	0.62*	0.68*	0.69*
	3	-	0.64*	0.62*	0.68*	0.70*
	4	-	-	0.62*	0.69*	0.70*

Table 3.6 The cross-validation correlations, averaged over the summer rainfall regions, for varying numbers of predictor and predictand modes, for single predictor variables used in the MOS equations. The highest mean correlation values are shaded, and values indicated with an asterisk are significant at the 95% confidence level.

Geopotential height at 850 hPa						
Number of modes		Predictor				
		2	3	4	5	6
Predictand	2	0.44*	0.39	0.34	0.31	0.28
	3	-	0.38	0.34	0.31	0.28
	4	-	-	0.35	0.30	0.26
Geopotential height at 700 hPa						
Number of modes		Predictor				
		2	3	4	5	6
Predictand	2	0.45*	0.41	0.36	0.37	0.28
	3	-	0.40	0.35	0.36	0.29
	4	-	-	0.37	0.35	0.25
Geopotential height at 500 hPa						
Number of modes		Predictor				
		2	3	4	5	6
Predictand	2	0.42	0.37	0.36	0.35	0.39
	3	-	0.36	0.35	0.33	0.37
	4	-	-	0.35	0.29	0.29
Geopotential height at 200 hPa						
Number of modes		Predictor				
		2	3	4	5	6
Predictand	2	0.33	0.26	0.21	0.16	0.07
	3	-	0.24	0.20	0.14	0.04
	4	-	-	0.20	0.13	-0.03
Humidity at 700 hPa						
Number of modes		Predictor				
		2	3	4	5	6
Predictand	2	0.08	0.03	0.38	0.35	0.35
	3	-	0.03	0.36	0.34	0.33
	4	-	-	0.37	0.37	0.37

Table 3.7 As in Table 3.6, but for pairs of predictor variables.

Geopotential Height at 700 hPa with Geopotential Height at 850 hPa						
Number of modes		Predictor				
		2	3	4	5	6
Predictand	2	0.45*	0.41	0.35	0.35	0.28
	3	-	0.40	0.35	0.34	0.28
	4	-	-	0.36	0.33	0.26

Geopotential Height at 700 hPa with Geopotential Height at 500 hPa						
Number of modes		Predictor				
		2	3	4	5	6
Predictand	2	0.44*	0.40	0.35	0.38	0.34
	3	-	0.39	0.35	0.36	0.33
	4	-	-	0.34	0.33	0.29

Geopotential Height at 700 hPa with Humidity at 700 hPa						
Number of modes		Predictor				
		2	3	4	5	6
Predictand	2	0.47*	0.45*	0.44*	0.42	0.38
	3	-	0.45*	0.43*	0.41	0.36
	4	-	-	0.43*	0.41	0.39

Geopotential Height at 700 hPa with Geopotential Height at 200 hPa						
Number of modes		Predictor				
		2	3	4	5	6
Predictand	2	0.40	0.39	0.36	0.37	0.36
	3	-	0.38	0.35	0.36	0.34
	4	-	-	0.37	0.34	0.35

Table 3.8 As in Table 3.6, but for three combined predictor variables.

Geopotential Height at 700 hPa and Humidity at 700 hPa with Geopotential Height at 850 hPa						
Number of modes		Predictor				
		2	3	4	5	6
Predictand	2	0.47*	0.44*	0.41	0.37	0.37
	3	-	0.43*	0.41	0.36	0.34
	4	-	-	0.41	0.38	0.36
Geopotential Height at 700 hPa and Humidity at 700 hPa with Geopotential Height at 500 hPa						
Number of modes		Predictor				
		2	3	4	5	6
Predictand	2	0.45*	0.42	0.41	0.39	0.36
	3	-	0.42	0.39	0.38	0.32
	4	-	-	0.39	0.36	0.36
Geopotential Height at 700 hPa and Humidity at 700 hPa with Geopotential Height at 200 hPa						
Number of modes		Predictor				
		2	3	4	5	6
Predictand	2	0.40	0.40	0.41	0.39	0.34
	3	-	0.40	0.40	0.38	0.33
	4	-	-	0.42	0.36	0.31

Table 3.9 As in Table 3.6, but for four combined predictor variables.

Geopotential Height at 700 hPa, Humidity at 700 hPa and Geopotential Height at 850 hPa with Geopotential Height at 500 hPa						
Number of modes		Predictor				
		2	3	4	5	6
Predictand	2	0.45*	0.43*	0.42	0.39	0.36
	3	-	0.42	0.42	0.38	0.35
	4	-	-	0.42	0.38	0.36
Geopotential Height at 700 hPa, Humidity at 700 hPa and Geopotential Height at 850 hPa with Geopotential Height at 200 hPa						
Number of modes		Predictor				
		2	3	4	5	6
Predictand	2	0.43*	0.42	0.42	0.42	0.38
	3	-	0.42	0.41	0.41	0.40
	4	-	-	0.42	0.41	0.39

Table 3.10 As in Table 3.6, but for all five combined predictor variables.

Geopotential Height at 700 hPa, Humidity at 700 hPa, Geopotential Height at 850 hPa and Geopotential Height at 500 hPa with Geopotential Height at 200 hPa						
Number of modes		Predictors				
		2	3	4	5	6
Predictand	2	0.43*	0.41	0.39	0.42	0.38
	3	-	0.41	0.38	0.41	0.38
	4	-	-	0.40	0.40	0.37

3.2.3 *Final selection*

The 700 hPa geopotential height field as predictor is associated with high skill for both the perfect prognosis and MOS recalibration models. The pressure gradients, also shown by earlier observed conditions (Taljaard *et al.*, 1969), is found in both the CSIRO 9 GCM simulated and NCEP reanalysis data (Figure 3.2). Therefore, given the close association between the fields, skilful recalibrated rainfall simulations may be possible owing to the predictor variable being well characterized by the GCM.

(A)

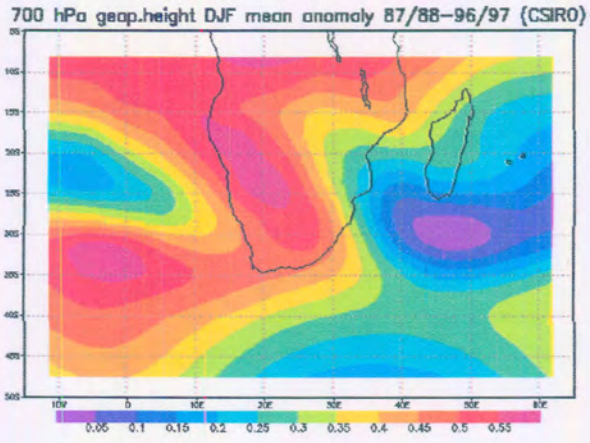

(B)

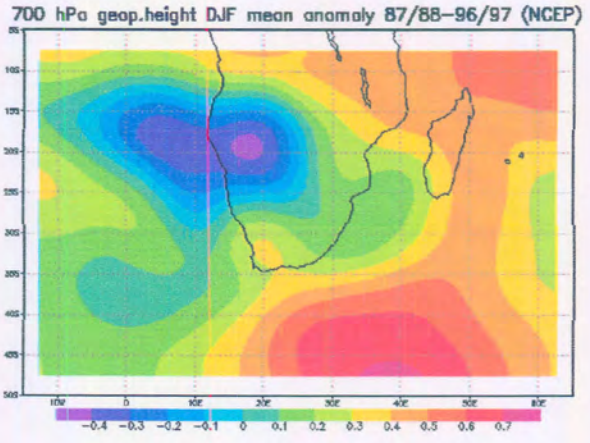

Figure 3.2 The mean 700 hPa geopotential height anomalies for December-January-February 1987/88 to 1996/97 for (a) the CSIRO 9 GCM climate and (b) the NCEP reanalysis climate.

3.3 Pattern Analysis

The objective of this section is to find, through the use of CCA, the common spatial anomaly structures between the two recalibration methods, and to investigate the predictor-predictand relationship over the given area. The predictor field is the DJF mean (1969/70 to 1996/97) 700 hPa geopotential height field, and the predictand the rainfall of the corresponding period. The results, presented below by means of maps and graphs, are discussed separately for MOS and perfect prognosis.

The g- and h-maps shown are canonical vectors whose components show the correlation at a specific location between the predictor (g-maps) or predictand (h-maps) and their respective canonical component time series presented in the accompanying graph. The hn-maps show the correlation between the rainfall indices and the time scores of the 700 hPa geopotential heights, the predictor field. The g-map describes the linear combination of the data that will contribute the largest fraction of predictability in the data set (Barnett and Preisendorfer, 1987). The significance of the correlation is tested at the 95% level using the Monte Carlo approach (Wilks, 1995). Strong correlations on the maps indicate areas where the association between the 700 hPa geopotential heights and rainfall is the greatest. The type of association between the predictor and predictand can be determined from the signs of the correlations and of the canonical component time series.

For both MOS and perfect prognosis, the correlation between the first canonical vector of the predictor and predictand (Figures 3.3 A and 3.4 A) is considerably higher than that of the second canonical vector. Emphasis will subsequently be on CCA mode 1, since the second mode provides only a small contribution to the predictability of the rainfall anomalies.

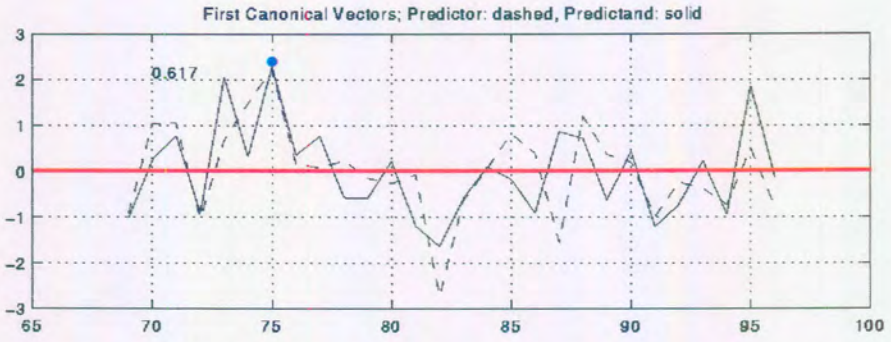

Figure 3.3 (A) MOS: The first canonical coefficients associated with the predictor and predictand. The dashed line indicates the canonical coefficient scores of the predictor, while the solid line represents the canonical coefficient scores of the predictand. The year "69" refers to the December 1969-January 1970-February 1970 season.

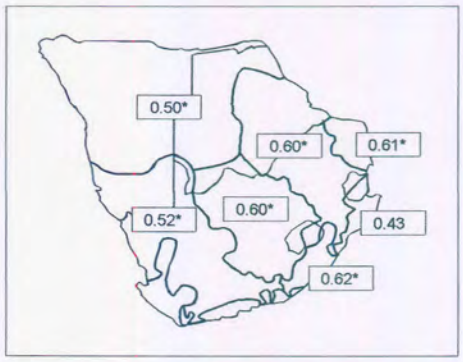

Figure 3.3 (B) MOS: The first canonical predictand map (hn-map) for DJF rainfall for each of the homogeneous rainfall regions over southern Africa. Values significant at the 95% level of confidence are indicated with an asterisk.

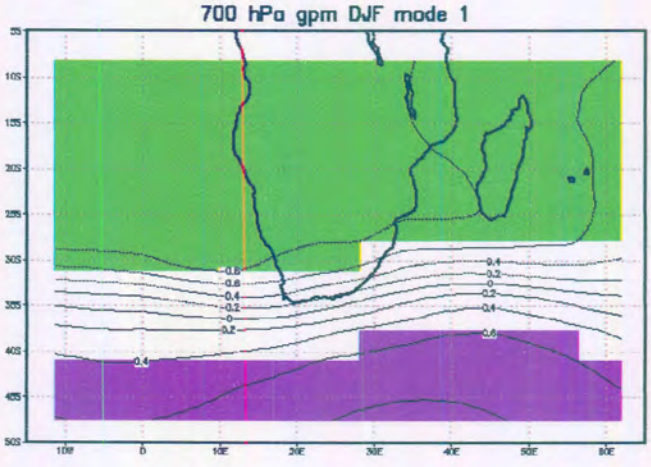

Figure 3.3 (C) MOS: The first canonical predictor map (g-map) for DJF geopotential height at 700 hPa. Areas of correlations significant at the 95% level are shaded green (negative) and purple (positive).

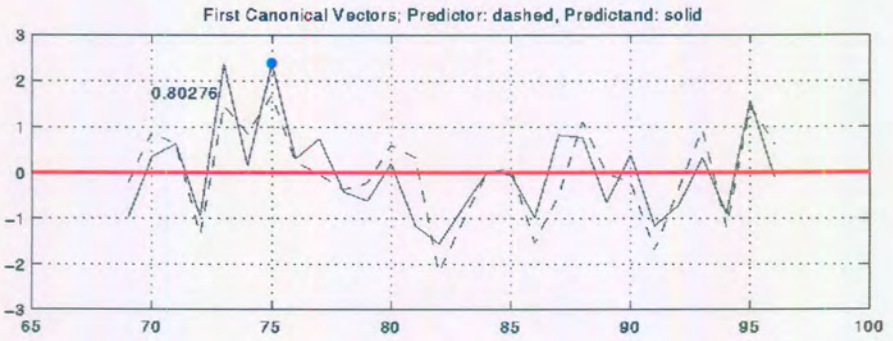

Figure 3.4 (A) Perfect prognosis: The first canonical coefficients associated with the predictor and predictand. The dashed line indicates the canonical coefficient scores of the predictor, while the solid line represents the canonical coefficient scores of the predictand. The year "69" refers to the December 1969-January 1970-February 1970 season.

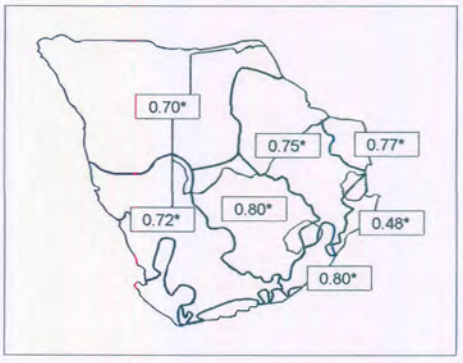

Figure 3.4 (B) Perfect prognosis: The first canonical predictand map (hn-map) for DJF rainfall for each of the homogeneous rainfall regions over southern Africa. Values significant at the 95% level of confidence are indicated with an asterisk.

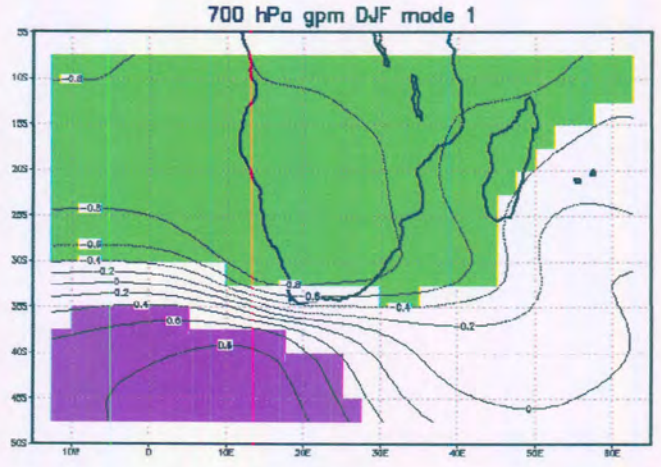

Figure 3.4 (C) Perfect prognosis: The first canonical predictor map (g-map) for DJF geopotential height at 700 hPa. Areas of correlations significant at the 95% level are shaded green (negative) and purple (positive).

3.3.1 Model Output Statistics

The area of significant negative correlation (95% level of confidence) between the simulated 700 hPa geopotential heights (Figure 3.3 C) and the canonical predictor scores (Figure 3.3 A, dashed line) includes most of the subcontinent with the exception of the southern parts of southern Africa, while the DJF rainfall indices for the summer rainfall region (Figure 3.3 B) are significantly and positively correlated with the predictand time series (Figure 3.3 A, solid line). Consider the 1975/76 DJF season (La Niña), indicated by a dot in Figure 3.3 A. The negative correlations over the subcontinent and the positive predictor time score in Figure 3.3 A indicate that the simulated 700 hPa geopotential heights are below average for the given season over land. The positive correlations in Figure 3.3 B and the positive predictand time score in Figure 3.3 A indicate that the rainfall is above average for the 1975/76 DJF season over the summer rainfall regions. A negative association between the simulated 700 hPa geopotential heights and rainfall is therefore implied, with anomalously lower (higher) than average 700 hPa geopotential heights over the interior accompanying anomalously wet (dry) conditions over the summer rainfall regions of southern Africa.

3.3.2 Perfect Prognosis

The greater part of the subcontinent and oceans to the east and west are included in the area of significant negative correlation between the 700 hPa geopotential heights of the reanalysis (Figure 3.4 C) and the canonical predictor scores (Figure 3.4 A, dashed line), with the exception of the southern coastal region. The DJF rainfall indices for the summer rainfall region (Figure 3.4 B) are significantly and positively correlated with the predictand time series (Figure 3.4 A, solid line). Following a similar analysis as for the simulated 700 hPa geopotential heights in MOS, a negative association between observed 700 hPa geopotential heights and rainfall is also implied, with anomalously lower (higher) 700 hPa geopotential heights over the interior accompanying anomalously wet (dry) conditions over the summer rainfall regions of southern Africa.

3.4 Summary and Discussion

Statistical recalibration models have been constructed for both a MOS and a perfect prognosis approach. The large-scale field that produced optimal recalibration models has been identified as the 700 hPa geopotential height field. The climatology of this field for both the GCM and reanalysis has been found to be in close agreement with the observed. In addition, both recalibration approaches are associated with similar circulation patterns that are responsible for drought and wet conditions over the subcontinent.

In the design of the optimal recalibration models, a large number of different potential predictors has been tested, which included the geopotential heights at 850, 700, 500 and 200 hPa, as well as the moisture field at 700 hPa. Owing to the close agreement between the dominant modes of variation associated with each potential predictor field, very similar skill scores have been obtained when using the 700 hPa geopotential height field on its own or combined as predictor in the CCA equations. Therefore, the addition of any field to the 700 hPa geopotential height field will not contribute to an improved recalibration model.

Pattern analyses of both the GCM and reanalysis data have shown that anomalously low (high) geopotential heights over the subcontinent, associated with anomalously high (low) heights to the south, are associated with wet (dry) conditions over southern Africa. This pattern is supported by analysis based on observations of rain (drought) producing systems (Tyson and Preston-Whyte, 2000), evidence that the observed large-scale structure and variability are well simulated by the GCM. The optimal recalibration models have therefore been found to be driven by a physically plausible predictor field. Next, it will be tested if these models can produce skilful rainfall simulations in a setting that is reminiscent of an operational forecast environment, and also to ascertain which one of the two models has the potential to produce the higher level of operational forecast skill.

CHAPTER 4

RETRO-ACTIVE SIMULATIONS

4.1 Introduction

MOS and perfect prognosis are used to recalibrate simulated large-scale circulation to categorized DJF rainfall over southern Africa. The perfect prognosis approach makes no attempt to correct for possible errors or biases of the CSIRO 9 GCM, but assumes that the GCM simulations are perfect. However, MOS directly includes the influence of the GCM's specific characteristics in the regression equations. Skill levels of the two recalibration techniques are compared and discussed in detail.

4.2 The Retro-Active Simulation Scheme

An ensemble of five GCM runs was forced with simultaneous observed SSTs over the 28 DJF seasons of 1969/70 to 1996/97. The resulting GCM fields are referred to as simulation mode fields. Large-scale circulation features are subsequently recalibrated retro-actively to observed regional rainfall for 10 DJF seasons, from 1987/88 to 1996/97. The training periods for the recalibration models for the 10-year MOS and perfect prognosis "forecasts" are as follows: A training period of 18 years is used to simulate the rainfall for 1987/88, 1988/89 and 1989/90; a training period of 21 years for 1990/91, 1991/92 and 1992/93; a training period of 24 years for 1993/94, 1994/95 and 1995/96; and finally a training period of 27 years for 1996/97. The predictor for the retro-active period is the simulated 700 hPa geopotential height field and the predictand is the set of southern Africa DJF rainfall indices.

The recalibrated and observed seasonal rainfall amounts are separated into three equi-probable groups for each of the seven summer rainfall regions. The three equi-probable

category boundaries are separately calculated for each of the four different climate periods of respectively 18, 21, 24 and 27 years involved in training the retro-active recalibration models. The upper tercile (associated with the highest rainfall years) is referred to as above-normal, the middle tercile as near-normal and the lower tercile (lowest rainfall years) as below-normal rainfall years.

4.3 Retro-active Simulations

The results of the retro-active MOS and perfect prognosis simulations for DJF 1987/88 to 1996/97 are presented in Table 4.1 and compared with the categorised observed rainfall.

Table 4.1 A Retro-active MOS and perfect prognosis simulations for December-January-February 1987/88 to 1990/91 for the seven summer rainfall regions of southern Africa, as well as the observed conditions. Blue areas indicate above-normal rainfall, green near-normal rainfall and red below-normal rainfall.

	MOS	Observed	Perfect Prognosis
1987/88	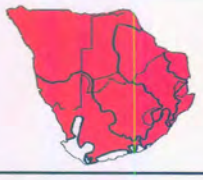		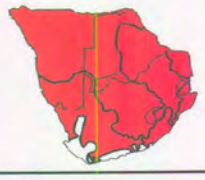
1988/89 La Niña			
1989/90		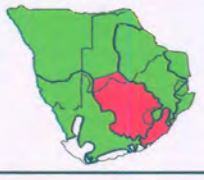	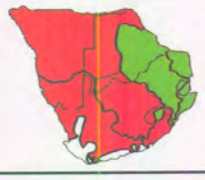
1990/91			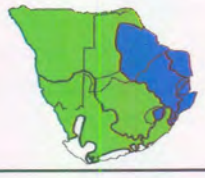

Table 4.1 B As for Table 4.1A, but for 1991/92 to 1996/97.

	MOS	Observed	Perfect Prognosis
1991/92 El Niño		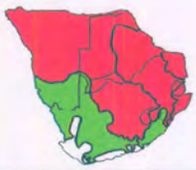	
1992/93			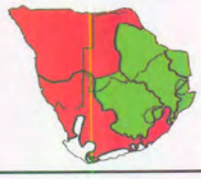
1993/94	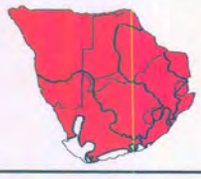		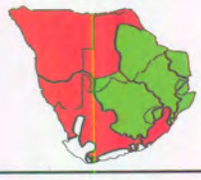
1994/95 El Niño	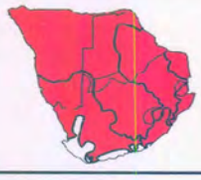	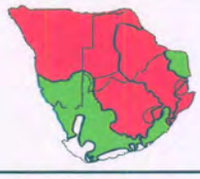	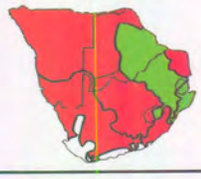
1995/96 La Niña	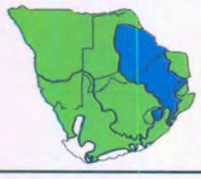		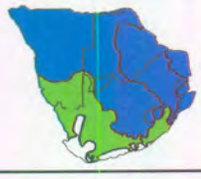
1996/97			

The MOS simulations show for nearly all DJF seasons an identical forecast for all regions. This is partly due to the coarse grid of the CSIRO 9 GCM over the region. Moreover, the categorical time series for the regions show that some of the retro-active simulations are in close proximity of category boundaries.

4.4 Skill Scores

The LEPS score and hit scores are used as measures of retro-active skill. The skill scores for each rainfall region (Figure 2.3) are depicted in Table 4.2, while Table 4.3 shows the hit scores for each DJF season.

Table 4.2 The LEPS and hit scores for each region for the ten year simulations.

	LEPS			Hit scores (out of 10 years)		
	MOS	Perfect Prognosis	MOS – Perf. Prog	MOS	Perfect Prognosis	MOS – Perf. Prog
Transkei	-2.1	-15.2	13.1	3	3	0
KwaZulu-Natal coast	52.5	18.2	34.3	5	4	1
Lowveld	-3.5	5.2	-8.7	3	4	-1
Northeastern Highveld	28.1	27.9	0.2	4	6	-2
Central interior	19.0	6.8	12.2	4	3	1
Western interior	-3.5	-67.8	64.3	3	1	2
N Namibia / W Botswana	34.1	-9.9	44.0	5	2	3

The reason why the hit scores are apparently more positive than LEPS, is because hit scores only account for hits or misses, while LEPS scores consider forecasts that are two categories out. The scores obtained using MOS are generally higher than those from perfect prognosis: the total number of hits for MOS is 27, and 23 for perfect prognosis. The LEPS scores obtained for MOS over the KwaZulu-Natal coast, the western interior and Northern Namibia/Western Botswana are substantially higher than that of perfect prognosis.

Table 4.3 The hit scores for each of the ten years.

	Hit scores (out of 7 regions)		
	MOS	Perfect Prognosis	MOS – Perf. Prog
1987/88	0	0	0
1988/89 La Niña	4	2	2
1989/90	5	5	0
1990/91	4	3	1
1991/92 El Niño	5	1	4
1992/93	3	3	0
1993/94	0	3	-3
1994/95 El Niño	4	2	2
1995/96 La Niña	2	4	-2
1996/97	0	0	0

The hit scores for MOS are in most cases the same or better than that of perfect prognosis, with the exception of 1993/94 and 1995/96. No hits are found from either approach for 1987/88 and 1996/97, and none for the MOS simulation of the 1993/94 season.

4.5 Case Studies

The MOS-recalibration outperforms the perfect prognosis over the 10-year retro-active period for most regions. In addition, the MOS hit scores are higher during 3 of the 4 ENSO years contained within the test period. Therefore, owing to the superiority of the MOS scheme over the perfect prognosis, the MOS is considered the preferred approach for doing statistical recalibration of the CSIRO 9 GCM simulations over southern Africa.

The spatial patterns for the first two CCA predictor modes for MOS are shown in Figure 4.1 and the corresponding canonical time scores in Figure 4.2. The GCM simulation of the 700 hPa geopotential height anomaly field for each of the retro-active simulated years are shown in Figure 4.3. From the pattern analysis for MOS (see Chapter 3), it has been shown that negative (positive) 700 hPa geopotential height anomalies over most of the continent, coincide with positive (negative) anomalies over the southern parts of the ocean, that give rise to favourable (unfavourable) rainfall conditions in the summer rainfall regions of southern Africa.

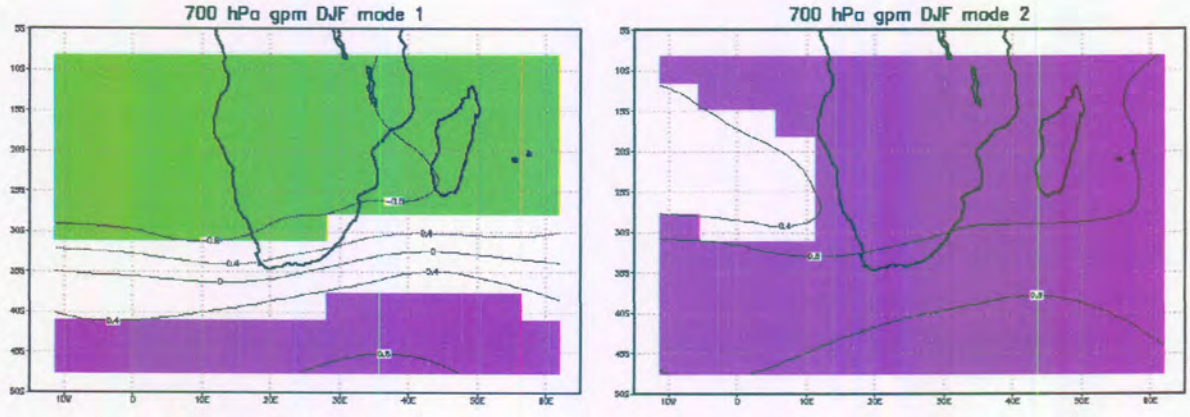

(A) **(B)**

Figure 4.1 The spatial patterns of (A) CCA mode 1 and (B) CCA mode 2, using the 700 hPa geopotential height field as predictor in the MOS recalibration. The areas significant at the 95% confidence level are shaded purple (positive) and green (negative).

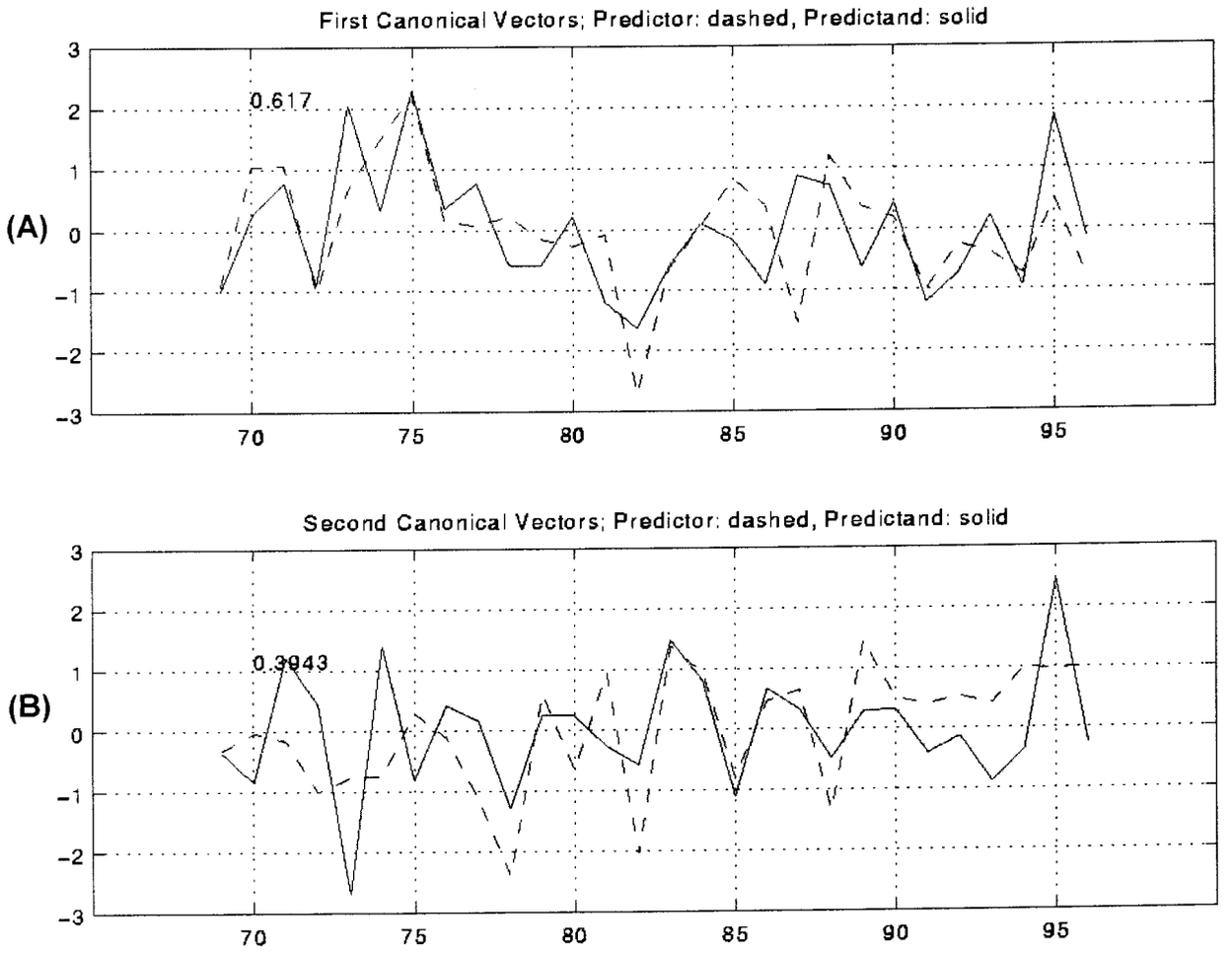

Figure 4.2 The time series of the (A) first canonical vector and (B) second canonical vector. The dashed line represents the predictor and the solid line the predictand. The x-axis depicts the year, i.e., 70 will refer to the DJF season of 1970/71.

4.5.1 ENSO years

The association between the first canonical vector and the ENSO signal can be seen in Figure 4.2 A: The El Niño events of 1969/70, 1972/73, 1982/83, 1991/92 and La Niña events of 1973/74, 1975/76 and 1995/96 are well represented in the time series of CCA mode 1. In addition, the series corresponds well with the SOI time series (0.65), a further indication that the first CCA mode is associated with ENSO. This strong association creates the opportunity for skilful seasonal rainfall simulations over southern Africa during ENSO years. The period of retro-active simulations contains four ENSO

events, namely the 1988/89 La Niña, the 1991/92 and 1994/95 El Niño events, and the La Niña of 1995/96.

During the first La Niña event of the retro-active period (1988/89), the simulated 700 hPa geopotential height anomaly field shows negative anomalies over the continent and adjacent ocean areas, and positive anomalies in the southeastern part of the ocean (Figure 4.3 B). This concurs with the spatial pattern of CCA mode 1 and the MOS recalibration consequently produced above-normal rainfall conditions for the region, which is in agreement with the observed wet conditions over the subcontinent.

The simulated 700 hPa geopotential height anomaly field for the 1991/92 El Niño event (Figure 4.3 E) shows positive anomalies over the continent and adjacent ocean areas, and negative anomalies in the southeastern part of the ocean. The height field for the El Niño event of 1994/95 similarly shows positive anomalies over the continent and adjacent ocean areas, but the area of negative anomalies is confined to the southwestern part of the ocean (Figure 4.3 H). Both patterns coincide to a large extent with the first CCA mode, and the MOS recalibration of rainfall conditions therefore produced below-normal conditions over the entire region for both cases. The observed rainfall also categorised into mainly below-normal for these two seasons.

The simulation of the 700 hPa geopotential height anomaly field for the weak La Niña event of 1995/96 (Figure 4.3 I) differs from the abovementioned episodes. Negative anomalies are found to the west of the continent and over the eastern parts, while weak positive anomalies occur over the remainder of the subcontinent. This pattern does not correspond distinctly with either of the two CCA modes. CCA mode 1 (associated with ENSO) dominates the MOS recalibrations, but the weakly negative SST anomalies in the eastern equatorial Pacific Ocean during the 1995/96 La Niña event are not sufficient to have produced a simulated anomaly pattern associated with above-normal rainfall conditions in most regions.

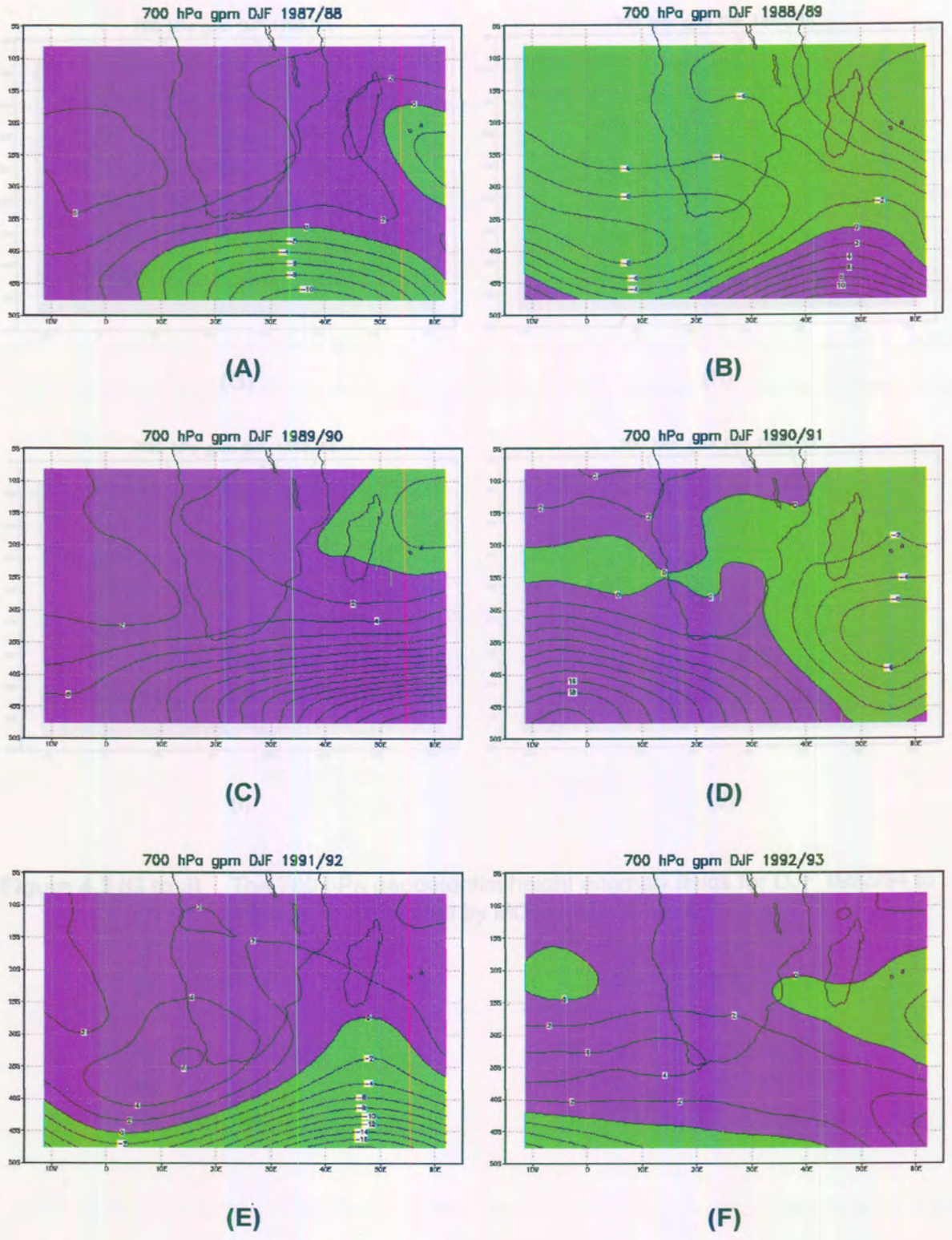

Figure 4.3 (A to F) The 700 hPa geopotential height anomaly fields for DJF 1987/88 to 1992/93 as simulated by MOS.

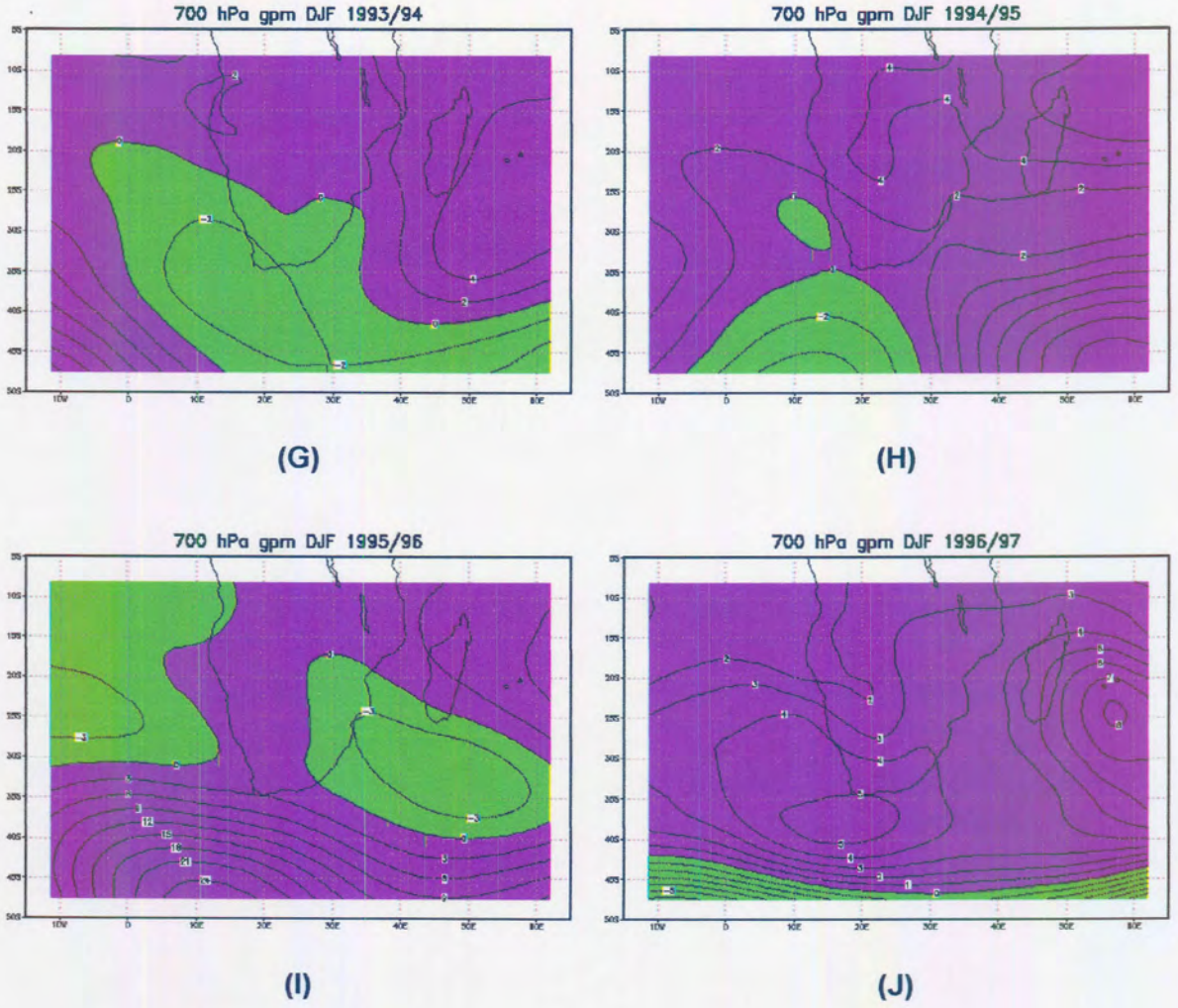

Figure 4.3 (G to J) The 700 hPa geopotential height anomaly fields for DJF 1993/94 to 1996/97 as simulated by MOS.

4.5.2 *The DJF 1987/88 season*

MOS recalibration produced below-normal rainfall conditions over the entire subcontinent, while the observed rainfall categorised mainly into above-normal (two of the regions are near-normal), resulting in the rainfall simulations being two categories out for the larger part of the region. It is evident that the simulated 700 hPa geopotential height anomaly pattern corresponds to that of the first mode's spatial pattern: positive anomalies are shown over the continent and adjacent ocean areas, with negative anomalies to the south (Figure 4.3 A), hence the below-normal MOS simulations.

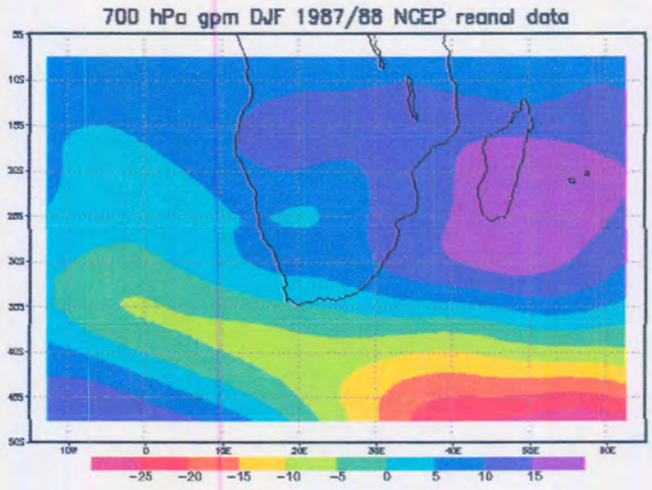

Figure 4.4 The 700 hPa geopotential height anomaly field for DJF 1987/88 from NCEP reanalysis data.

Figure 4.4 shows the 700 hPa geopotential height anomaly field from the reanalysis data. These observed conditions show positive anomalies in the east and negative anomalies extending from the southeast into the ocean areas to the west of the continent. From the observed conditions for these three months, as given by the South African Weather Bureau summary (Weather Bureau 1987; 1988), it is evident that

tropical disturbances in the Indian Ocean influenced the rainfall over a large part of the region during this period. Moist air in the wake of the tropical cyclone Doaza started off the wet conditions. Exceptionally heavy rains also occurred over the central interior of the region (Weather Bureau, 1988), associated with a tropical-temperate trough that prevailed for several days during February 1988 (Crimp et al., 1997; Todd and Washington, 1999). These rains caused flooding over many parts of the country and overflowing rivers and dams added to the damage. The cold fronts hitting the southwestern Cape and the position of the tropical-temperate trough over the interior are reflected in the negative 700 hPa geopotential height anomalies of Figure 4.4. These systems caused the positive height anomalies normally associated with drought conditions to be further to the east, resulting in the observed high rainfall totals over the central and western interior during the 1987/88 season. The tropical disturbances, which mostly occur over a relatively small area, were not simulated by the GCM. The reason can be found in the fact that GCMs presently are not run at a horizontal resolution fine enough to produce meaningful simulations of tropical disturbances, especially over the southwestern Indian Ocean. Even with a GCM resolution close to 1 degree, the mean simulated tropical storm frequency is only about half of the number observed (Vitart and Stockdale, 2001).

4.5.3 The DJF 1989/90 season

The recalibration for this season produced the highest retro-active skill scores for the non-ENSO seasons. The hit score for MOS is 5 out of a possible 7. The simulated 700 hPa geopotential height anomaly field is shown in Figure 4.3 C. Nearly the entire area under consideration has simulated positive height anomalies, with higher values in the southeastern quadrant. This pattern agrees to some extent with that of the second CCA mode. For this mode, anomalously higher 700 hPa geopotential heights over the KwaZulu-Natal coast, the Lowveld and the northeastern Highveld are associated with conditions that are favourable for rainfall, which is in agreement with the MOS simulation of near-normal rainfall.

4.5.4 The DJF 1993/94 season

The recalibrated MOS rainfall for this season shows below-normal conditions over the entire region, while the observed conditions are near-normal to above-normal. The recalibration is, therefore, two categories out for the western interior, the central interior and the Transkei regions. The reason for this can be found in the simulated 700 hPa geopotential height anomaly field (Figure 4.3 G), showing negative anomalies extending from the south over the southern parts of the continent and the western ocean areas. This pattern is reminiscent of the north-south anomaly pattern of CCA mode 1, but for dry conditions. This mode dominates the simulation in terms of variance explained. This season's weakly positive SST anomalies in the eastern equatorial Pacific Ocean may therefore have produced a below-normal rainfall recalibrated MOS simulation in the region.

4.6 Summary and Discussion

Retro-active rainfall simulations for the summer rainfall regions of southern Africa, using two statistical recalibration schemes, have been presented. These recalibrated "forecasts" have been derived from simulation mode CSIRO 9 GCM circulation output, and have been done for an independent 10-year retro-active test period that covers most of the 1990s. The two statistical recalibration methods that have been used here are MOS and perfect prognosis, of which the former has produced a higher level of skill over the test period than the latter. Notwithstanding the higher skill levels of the MOS model, both approaches have produced recalibrated rainfall simulations that have outscored chance.

Most of the rainfall simulations during ENSO years have been found to be skilful, which is a result of the dominant CCA mode in the recalibration equations being in close agreement with the eastern equatorial SST variability. Some of the rainfall simulations

during non-ENSO years have also been successful. Those seasonal rainfall amounts that have been poorly recalibrated are due to a GCM-simulated large-scale anomaly pattern for that season that has not been represented by the dominant modes of the CCA recalibration equations, and will in most cases produce inaccurate rainfall forecasts as a result.

CHAPTER 5

SUMMARY AND CONCLUSIONS

Many aspects of human life are influenced by the variability of climate on seasonal-to-interannual time scales. The ability to predict these climate variations skilfully is one of the most important elements for planning future activities in modern societies in an intelligent manner. Both empirically- and physically based models are used as prediction methods to forecast seasonal climate variations. Until the recent past, mostly statistical models had been used in seasonal forecasts for southern Africa. However, the use of general circulation models (GCMs) has become essential for seasonal forecasting, since the ocean-atmosphere interactions responsible for the interannual rainfall variability over southern Africa are non-linear and cannot be taken into account by statistical models which are mostly linear. The direct output from GCMs on an inter-annual to intra-annual time scale is, however, inadequate for assessing land-surface impacts on a regional scale. Consequently, recalibration techniques have emerged as a means of relating large-scale GCM output to surface variables such as rainfall.

Simulation mode large-scale GCM output has been recalibrated to equi-probable austral summer rainfall terciles for southern Africa. From this, measures of skill have been calculated over a 10-year independent test period to establish the difference in skill levels of two statistical recalibration techniques. The purpose of the skill comparison is to establish if a method that uses much less computer resources can produce equally skilful forecasts than a much more elaborate and expensive method that takes the systematic errors of the GCM into account. The objective has been met, and the findings of the research are summarized below.

5.1 Compiling the recalibration equations

1. Cross-validation sensitivity tests have been performed over a 28-year climate period to design an optimal model for each of the two recalibration methods, MOS and perfect prognosis. Simulation mode output from the CSIRO9 GCM has been used as predictor in the development of the MOS equations, and reanalysis data for the development of the perfect prognosis equations. Raw GCM output has been used to test the recalibration performance of the two techniques over a 10-year independent test period.

2. Of the various potential predictors considered in designing the optimal set of equations, the 700 hPa geopotential height field has been identified as the best predictor in both sets of recalibration equations. The percentage explained variance of the GCM and observed predictor field is respectively 75.1% and 79.9%.

3. Owing to the close agreement between the dominant modes of variation associated with each potential predictor field, it has been found that the addition of any other potential predictor field to the selected 700 hPa geopotential height field has not contributed to any significant improvement in the skill of the recalibration equations.

4. The pressure gradients in the 700 hPa geopotential height field, also shown by earlier observed conditions, is found in both the CSIRO 9 GCM simulated and NCEP reanalysis data.

5.2 Pattern Analyses

5. Pattern analyses, based on both sets of CCA recalibration equations, have

demonstrated that anomalously low (high) 700 hPa geopotential heights over the subcontinent are associated with wet (dry) conditions over land. This association is supported by observational evidence, and illustrates that the atmospheric large-scale structure and variability are also well simulated by the GCM.

6. The dominant mode of the recalibration equations has been found to be associated with ENSO: dry (wet) conditions over land are associated with El Niño (La Niña) events.

5.3 Recalibrated rainfall simulations

7. Of the two statistical methods used to recalibrate the simulated large-scale GCM circulation to seasonal rainfall categories, the MOS technique has produced the higher forecast skill over the independent test period.

8. Notwithstanding the slightly higher skill levels of the MOS technique, both MOS and perfect prognosis have produced rainfall forecasts that outscored chance.

9. Usable forecast skill scores have been obtained for the KwaZulu-Natal, northeastern Highveld and Northern Namibia/Western Botswana regions using either MOS or perfect prognosis.

10. MOS forecasts have produced useful hit scores for 3 out of the 4 ENSO rainfall seasons during the independent test period, which is a manifestation of the association between ENSO and the dominant mode of the forecast equations. In addition, the rainfall forecasts for some of the non-ENSO years, namely 1989/90 and 1990/91, have been made successfully.

11. Poor forecast skill is a result of a mismatch between the GCM-simulated 700 hPa

height anomaly field and the dominant CCA modes of the recalibration equations.

Even though the simulation-MOS data presented in this dissertation do not explicitly hold any operational forecasting utility owing to the simultaneity of the SST forcing field and the rainfall season, it is necessary to note the following regarding the potential usefulness of the recalibration schemes presented here in an operational forecast environment that implies a lead-time: Given evidence that the large-scale structure and variability of the large-scale fields are well characterized by the GCM driven with different SST forcing fields that involves a lead-time, skilful MOS real-time rainfall forecasts over southern Africa are possible (Landman and Goddard, 2002). Moreover, owing to the most dominant mode in the recalibration equations being closely related to ENSO, and the fact that high persistence forecast skill exists in the eastern equatorial Pacific Ocean during its peak season (e.g., Barnston *et al.*, 1994; Landman and Mason, 2001; Mason and Mimmack, 2002), the MOS recalibration should produce skilful rainfall forecasts at lead-times of at least a few months.

The CSIRO9 GCM large-scale circulation has been successfully recalibrated to summer rainfall categories over southern Africa using two recalibration techniques, namely MOS and perfect prognosis. It has been found that the set of equations that has both been developed and tested using GCM output (MOS approach) has produced higher skill levels than the equations developed on observed data (perfect prognosis approach). However, the perfect prognosis technique should also be able to produce usable seasonal rainfall forecasts over southern Africa in an operational forecast environment hampered by the lack of computing resources.

REFERENCES

Barnett, T.P. and R.W. Preisendorfer (1987) Origins and levels of monthly and seasonal forecast skill for United States air temperature determined by canonical correlation analysis. *Monthly Weather Review*, **115**, 1825-1850.

Barnett, T.P., M. Latif, N. Graham, M. Flugel, S. Pazan and W. White (1993) ENSO and ENSO-related predictability: Part 1 - Prediction of equatorial Pacific sea-surface temperatures with a hybrid coupled ocean-atmosphere model. *Journal of Climate*, **6**, 1545-1566.

Barnett, T.P., L. Bengtsson, K. Arpe, M. Flügel, N. Graham, M. Latif, J. Ritchie, E. Roeckner, U. Schlese, U. Schulzweida and M. Tyree (1994) Forecasting global ENSO-related climate anomalies. *Tellus 46A*, **4**, 381-397.

Barnett, T.P. (1995) Monte Carlo climate forecasting. *Journal of Climate*, **8**, 1005-1022.

Barnston, A.G. and C.F. Ropelewski (1992) Prediction of ENSO using canonical correlation analysis. *Journal of Climate*, **5**, 1316-1345.

Barnston, A.G. and H.M. van den Dool (1993) A degeneracy in cross-validated skill in regression-based forecasts. *Journal of Climate*, **6**, 963-977.

Barnston, A.G. (1994) Linear statistical short-term climate predictive skill in the Northern Hemisphere. *Journal of Climate*, **7**, 1513-1564.

Barnston, A.G, H.M. van den Dool, S.E. Zebiak, T.P. Barnett, M. Ji, D.R. Rodenhuis, M.A. Cane, A. Leetmaa, N.E. Graham, C.R. Ropelewski, V.E. Kousky, E.A.

O'Lenic and R.E. Livezey (1994) Long-lead seasonal forecasts - where do we stand?, *Bulletin of the American Meteorological Society*, **66**, 2097-2114.

Barnston, A.G. and T.M. Smith (1996) Specification and prediction of global surface temperature and precipitation from global SST using CCA. *Journal of Climate*, **9**, 2660-2697.

Bengtsson L, K Arpe, E Roeckner and U Schulzweida (1996) Climate predictability experiments with a general circulation model. *Climate Dynamics,* **12**, 261-278.

Blanke, B., J.D. Neelin and D. Gutzler (1997) Estimating the effect of stochastic wind stress forcing on ENSO irregularity. *Journal of Climate*, **10**, 1473-1486.

Buchmann, J., J. Peagle, L.E. Buja and R.E. Dickenson (1990) The effect of tropical Atlantic heating anomalies upon GCM rain forecasts over the Americas. *Journal of Climate.*, **3**, 189-208.

Charles, S.P., B.C. Bates, P.H. Whetton and J.P. Hughes (1999) Validation of downscaling models for changed climate conditions: case study of southwestern Australia. *Climate Research*, **12**, 1-14.

Chu, P. and Y. He (1994) Long-range prediction of Hawaiian winter rainfall using canonical correlation analysis. *International Journal of Climatology*, **14**, 659-669.

Crimp, S. J., S.C. van den Heever, P.C. D'Aberton, P.D. Tyson and S.J. Mason (1997) Mesoscale Modelling of Tropical-Temperate Troughs and Associated Systems over Southern Africa. *Report to the Water Research Commission*, WRC 595/1/97, 395 pp.

Cubasch, U., H. von Storch, J. Waszkewitz and E. Zorita (1996) Estimates of climate

change in southern Europe using different downscaling techniques. *Max Planck Institut für Meteorologie, Report No. 183*, 46 pp.

Fox-Rabinovitz, M.S., G.L. Stenchikov, M.J. Suarez and L.L. Takacs (1997) A finite-difference GCM dynamical core with a variable-resolution stretched grid. *Monthly Weather Review*, **125**(11), 2943-2968.

Glahn, H.R. and D.A. Lowry (1972) The use of model output statistics (MOS) in objective weather forecasting. *Journal of Applied Meteorology*, **11**, 1203-1211.

Gordon, H.B. (1981) Flux formulation of the spectral atmospheric equations suitable for use in long-term climate modeling. *Monthly Weather Review*, **109**, 56-64.

Graham, N.E., J. Michaelsen, and T.P. Barnett (1987a) An investigation of the El Niño-Southern Oscillation cycle with statistical models. 1. Predictor field characteristics. *Journal of Geophysical Research*, **92**, 14251-14270.

Graham, N.E., J. Michaelsen, and T.P. Barnett (1987b) An investigation of the El Niño-Southern Oscillation cycle with statistical models. 2. Model results. *Journal of Geophysical Research*, **92**, 14271-14289.

Graham, N.E. and T.P. Barnett (1995) ENSO and ENSO related predictability, Part II: Northern hemisphere 700 mb height predictions based on a hybrid coupled ENSO model. *Journal of Climate*, **8**, 544-549.

Grolier Multimedia Encyclopedia (1998) Version 10.0, *Grolier Interactive Inc.*

Harrison, M.S.J. (1994) Ensembles, higher-resolution models and future computing power - a personal view. *Weather*, **49**, 398-406.

Hastenrath, S. (1990a) Prediction of Northeast Brazil rainfall anomalies. *Journal of Climate*, **3**, 893-904.

Hastenrath, S. (1990b) Tropical climate prediction: A progress report. *Bulletin of the American Meteorological Society*, **71**, 819-825.

Hastenrath, S. (1991) *Climate Dynamics of the Tropics.* Kluwer Academic Publishers, Dordrecht. 488 pp.

Hay, L.E., G.J. McCabe, D.M. Wolock and M.A. Ayers (1992) Use of weather types to disaggregate General Circulation Model predictions. *Journal of Geophysical Research*, **97**, 2781-2790.

Haywood, J.M., V. Ramaswamy and L.J. Donner (1997) A limited-area-model case study of the effects of sub-grid scale variations in relative humidity and cloud upon the direct radiative forcing of sulfate aerosol. *Geophysical Research Letters*, **24**(2), 143-146.

Hunt, B.G. (1997) Prospects and problems for multi-seasonal predictions: some issues arising from a study of 1992. *International Journal of Climatology*, **17**, 137-154.

Huth, R. (1999) Statistical downscaling in central Europe: evaluation of methods and potential predictors. *Climate Research*, **13**, 91-101.

Jackson, J.E. (1991) *A User's Guide to Principal Components*, Wiley, New York, 569 pp.

Jury, M. R. and B. M. R. Pathack (1991) A study of climate and weather variability over the tropical southwest Indian Ocean. *Meteorology and Atmospheric Physics*, **47**, 37-48.

Jury, M.R. (1993) A preliminary study of climatological associations and characteristics of tropical cyclones in the SW Indian Ocean. *Meteorology and Atmospheric Physics*, **51**, 101-115.

Jury, M. R. (1996) Regional teleconnection patterns associated with summer rainfall over South Africa, Namibia and Zimbabwe. *International Journal of Climatology*, **16**, 135-153.

Jury, M.R., H.M. Mulenga and S.J. Mason (1999) Exploratory long-range models to estimate summer climate variability over southern Africa. *Journal of Climate*, **12**, 1892-1899.

Kalnay, E., M. Kanamitsu, R. Kistler, W. Collins, D. Deaven, L. Gandin, W. Iredell, S. Saha, G. White, J. Woollen, Y. Zhu, M. Chelliah, W. Ebisuzaki, W. Higgens, J. Janowiak, K.C. Mo, C. Ropelewski, J. Wang, A. Leetmaa, R. Reynolds, R. Jenne and J. Dennis (1996) The NCEP/NCAR 40-year reanalysis project. *Bulletin of the American Meteorological Society*, **77**, 437-471.

Kirtman, B.P., J. Schukla, B. Huang, Z. Zhu and E.K. Schneider (1997) Multiseasonal predictions with a coupled tropical ocean global atmosphere system. *Monthly Weather Review*, **125**, 789-808.

Kleeman, R. (1999) Forecast of NINO3 using a low order coupled ocean-atmosphere model. *Experimental Long-Lead Forecast Bulletin*, **8**, 7-9.

Klopper, E. (1999) The use of seasonal forecasts in South Africa during the 1997/98 rainfall season. *Water SA*, **25**, 311-316.

Klopper, E. and A.G. Bartman (2001)Forecasts and commercial agriculture: a survey of user needs in South Africa. *Coping with Climate Variability: The Use of*

Seasonal Climate Forecasts in Southern Africa, *Eds: K. O'Brien and H.C. Vogel*, Ashgate Publishing Company, **Chapter 10**, 171-183.

Klopper, E. and W.A. Landman (2002) A retro-active perspective on seasonal forecasts for southern Africa during the mid-summer months of the 1990s. Submitted to *Meteorological Applications*.

Kruger, A.C. (1999) The influence of the decadal-scale variability of summer rainfall on the impact of El Niño and La Niña events in South Africa. *International Journal of Climatology*, **19**, 59-68.

Kumar, A. and M.P. Hoerling (1995) Prospects and limitations of seasonal atmospheric GCM predictions. *Bulletin of the American Meteorological Society*, **76**, 335-345.

Landman, W.A. and S.J. Mason (1999) Change in the association between Indian Ocean sea-surface temperatures and summer rainfall over South Africa and Namibia. *International Journal of Climatology*, **19**, 1477-1492.

Landman, W.A. and S.J. Mason (2001) Forecasts of near-global sea-surface temperatures using canonical correlation analysis. *Journal of Climate*, **14**, 3819-3833.

Landman, W.A., S.J. Mason, P.D. Tyson and W.J. Tennant (2001a) Retro-active skill of multi-tiered forecasts of summer rainfall over southern Africa. *International Journal of Climatology*, **21**, 1-19.

Landman, W.A., S.J. Mason, P.D. Tyson and W.J. Tennant (2001b) Statistical Downscaling of GCM simulations to stream flow. *Journal of Hydrology*, **252**, 221-236.

Landman, W.A. and L. Goddard (2002) Statistical recalibration of GCM forecasts over southern Africa using model output statistics. *Journal of Climate*, accepted.

Levey, K.M. (1993) *Intra-seasonal Oscillations of Convection over Southern Africa.* Unpublished M.Sc. Dissertation, University of Cape Town.

Lindesay, J.A. (1988) South African rainfall, the Southern Oscillation and a southern hemisphere semi-annual cycle. *Journal of Climate*, **8**, 17-30.

Livezey, R.E. and W.Y. Chen (1983) Statistical field significance and its determination by Monte Carlo techniques. *Monthly Weather Review*, **111**, 46-59.

Livezey, R.E. (1990a) Variability of skill of long-range forecasts and implications for their use and value. *Bulletin of the American Meteorological Society*, **71**, 300-309.

Livezey, R.E. (1990b) Seasonal Predictability and Prediction in the Extra-tropics. *World Meteorological Organisation: Programme on Long-Range Forecasting Research Report No. 13*, World Meteorological Organisation, 15-19.

Livezey, R.E., M. Masutani and M. Ji (1996) SST-forced seasonal simulation and prediction skill for versions of the NCEP/MRF model. *Bulletin of the American Meteorological Society*, **77**, 507-517.

Main, J.P.L. and B.C. Hewitson (1995) Regionalisation of daily precipitation in Botswana 1972-1989. *South African Geographical Journal*, **77**, 51-55.

Makarau, A. and M.R. Jury (1997) Predictability of Zimbabwe summer rainfall. *International Journal of Climatology*, **17**, 1421-1432.

Mason, S.J. (1995) Sea-surface temperature - South African rainfall associations, 1910-1989. *International Journal of Climatology*, **15**, 119-135.

Mason, S.J., A.M. Joubert, C. Cosijn and S.J. Crimp (1996) Review of seasonal forecasting techniques and their applicability to Southern Africa. *Water SA*, **22**, 203-209.

Mason, S. J. and M. R. Jury, (1997) Climate variability and change over southern Africa: a reflection on underlying processes. *Progress in Physical Geography*, **21**, 23-50.

Mason, S.J. (1998) Seasonal forecasting of South African rainfall using a non-linear discriminant analysis model. *International Journal of Climatology*, **18**, 147-164.

Mattes, M. and S.J. Mason (1998) Evaluation of a seasonal forecasting procedure for Namibian rainfall. *South African Journal of Science*, **94**, 183-185.

McGregor, J.L., H.B. Gordon, I.G. Watterson, M.R. Dix and L.D. Rotstayn (1993) The CSIRO 9-level Atmospheric General Circulation Model. CSIRO *Division of Atmospheric Research Technical Paper No 26.* 89 pp.

Michaelsen, J. (1987) Cross-validation in statistical climate forecast models. *Journal of Climate and Applied Meteorology*, **26**, 1589-1600.

Moura, A.D. (1994) Prospects for seasonal-to-interannual climate prediction and applications for sustainable development. *WMO Bulletin*, **43**, 207-215.

Murphy, J. (1999) An evaluation of statistical and dynamical technique for downscaling local climate. *Journal of Climate*, **12**, 2256-2284.

Murphy, J. (2000) Predictions of climate change over Europe using statistical and dynamical downscaling techniques. *International Journal of Climatology*, **20**, 489-501.

National Department of Agriculture (1997) *A Profile of Agriculture in South Africa*. CTP Book Printers, Cape Town. 32 pp.

Nicholson, S. E. and D. Entekhabi (1987) Rainfall variability in equatorial and southern Africa: relationships with sea surface temperatures along the southwestern coast of Africa. *Journal of Climate and Applied Meteorology*, **26**, 561-578.

Palmer, T.N., R. Mureau and T. Molteni (1990) The Monte Carlo forecast. *Weather*, **45**, 198-207.

Palmer, T.N. and L.T. Anderson (1994) The prospects for seasonal forecasting. *Quaterly Journal of the Royal Meteorological Society*, **120**, 755-793.

Perica, S. and E. Foufoula-Georgiou (1996) A model for multiscale disaggregation of spatial rainfall based on coupling meteorological and scaling descriptions. *Journal of Geophysical Research*, **101**, 26347-26361.

Pierce, D.W. (1996) The Hybrid Coupled Model Version 3: Technical Notes. *SIO Reference Series No 96-27*, Scripps Institution of Oceanography, University of California, San Diego.

Pollard, D. and S.L. Thompson (1997) Driving a high-resolution dynamic ice-sheet model with GCM climate: ice-sheet initiation at 116 000 BP. *Annals of Glaciology*, **25**, 296-304.

Posch, M. (1994) Development of a weather generator for Finland II. *The Finnish*

Research Programme on Climate Change: Second Progress Report, 323-328.

Potts, J.M., C.K. Folland, I.T. Jolliffe and D. Sexton (1996) Revised 'LEPS' scores for assessing climate model simulations and long-range forecasts. *Journal of Climate*, **9**, 34-53.

Preisendorfer, R.W. (1988) *Principal Component Analysis in Meteorology and Oceanography*, Elsevier, New York, p. 425.

Racsko, P., L. Szeidl and M. Semenov (1991) A serial approach to local stochastic weather models. *Ecological Modelling*, **57**, 27-41.

Rautenbach, C.J. de W. (1999) *Introduction of a hybrid vertical co-ordinate to an Atmospheric General Circulation model.* PhD Thesis, University of Pretoria.

Rautenbach, C.J.de W. and I.N. Smith (2001) Teleconnections between global sea-surface temperatures and the interannual variability of observed and model simulated rainfall over southern Africa. *Journal of Hydrology*, **254**, 1-15.

Reason, C.J.C. and J.R.E. Lutjeharms (1998) Variability of the south Indian Ocean and implications for southern African rainfall. *South African Journal of Science*, **94**, 115-123.

Reason, C.J.C. (1999) Interannual warm and cool events in the subtropical/mid-latitude south Indian Ocean region. *Geophysical Research Letters*, **26**, 215-218.

Rocha, A. and I. Simmonds (1997) Interannual variability of south-eastern African summer rainfall. Part I: relationships with air-sea interaction processes. *International Journal of Climatology*, **17**, 235-266.

Ropelewski, C.F. and M.S. Halpert (1987) Global and regional scale precipitation patterns associated with the El Niño/Southern Oscillation. *Monthly Weather Review,* **115**, 1606-1626.

Ropelewski, C.F. and M.S. Halpert (1989) Precipitation patterns associated with the high index of the Southern Oscillation. *Journal of Climate*, **2**, 268-284.

Rummukainen, M. (1997) *Methods for Statistical Downscaling of GCM Simulations*. Swedish Meteorological and Hydrological Institute. Report nr RMK 80. 29 pp.

Schneider, E.K., B. Huang, Z. Zhu, D.G. De Witt, J.L. Kinter, B. Kirtman and J. Shukla (1999) Ocean data assimilation, initialization, and predictions of ENSO with a coupled GCM. *Monthly Weather Review*, **127**, 1187-1207.

Schulze, G.C. (1986) South African rainfall related to warm and cold events. *2nd International Conference on Southern Hemisphere Meteorology*, American Meteorological Society, 465-467.

Semonov, M.A. and E.M. Barrow (1997) Use of a stochastic weather generator in the development of climate change scenarios. *Climatic Change*, **35**, 397-414.

Shinoda, M. and R. Kawamura (1996) Relationships between rainfall over semi-arid southern Africa, geopotential heights, and sea surface temperatures. *Journal of the Meteorological Society of Japan*, **74**, 21-36.

Smith, T.M. and R.E. Livezey (1999) GCM Systematic Error Correction and Specification of the Seasonal Mean Pacific-North America Region Atmosphere from Global SSTs. *Journal of Climate*, **12**, 273-288.

Smith, T.M., R.W. Reynolds, R.E. Livezey and D.C. Stokes (1996) Reconstruction of

historical sea surface temperatures using empirical orthogonal functions. *Journal of Climate*, **9**, 1403-1420.

Stern, P.C. and E. Easterling, Eds. (1999) *Making Climate Forecasts Matter.* National Academy Press, Washington D.C., 164 pp.

Syu, H-H., J.D. Neelin and D. Gutzler (1995) Seasonal and interannual variability in a hybrid coupled model GCM. *Journal of Climate*, **8**, 2121-2143.

Taljaard J.J., H. van Loon, H.L. Crutcher and R.L. Jenne (1969) *Climate of the Upper Air Southern Hemisphere: Volume 1.* A joint production of the National Center for Atmospheric Research, the National Weather Records Center and the U.S. Department of Defence.

Tatsuoka, M. (1988) *Multivariate Analysis*, Macmillan, New York, 241-249.

Todd, M. and R. Washington (1999) Circulation anomalies associated with tropical-temperate troughs in southern Africa and the south west Indian Ocean, *Climate Dynamics*, **15**, 937-951.

Toth, Z. and E. Kalnay (1993) Ensemble forecasting at NMC: the generation of perturbations. *Bulletin of the American Meteorological Society*, **74**, 2317-2330.

Tyson, P.D. (1986) *Climate Change and Variability in Southern Africa.* Oxford University Press, Cape Town, 220pp.

Tyson, P.D. and R.A. Preston-Whyte (2000) *The Weather and Climate of southern Africa*. Oxford University Press, Cape Town, 396pp.

Vitart, F. and T.N. Stockdale (2001) Seasonal forecasting of tropical storms using

coupled GCM integrations. *Monthly Weather Review*, **129**, 2521-2537.

Von Storch, H. and A. Navarra (Eds) (1995) *Analysis of Climate Variability. Application of Statistical Techniques*, Springer-Verlag, Berlin, p. 334.

Walker, N. D. (1990) Links between South African summer rainfall and temperature variability of the Agulhas and Benguela currents systems. *Journal of Geophysical Research*, **95**, 3297-3319.

Ward, M.N. and C.K. Folland (1991) Prediction of seasonal rainfall in the north Nordeste of Brazil using eigenvectors of sea-surface temperature. *International Journal of Climatology*, **11**, 711-743.

Weather Bureau (1987) Newsletter December 1987. *RSA Government Printers*, 24 pp.

Weather Bureau (1988) Newsletter February 1988. *RSA Government Printers*, 28 pp.

Wigley, T.M.L., P.D. Jones, K.R. Briffa and G. Smith (1990) Obtaining sub-grid scale information from coarse-resolution general circulation model output. *Journal of Geophysical Research*, **95**, 1943-1953.

Wilby, R.L. and T.M.L. Wigley (2000) Precipitation Predictors for Downscaling: Observed and General Circulation Model Relationships. *International Journal of Climatology*, **20**, 641-661.

Wilks, D.S. (1989) Statistical specification of local surface weather elements from large-scale information. *Theoretical and Applied Climatology*, **40**, 119-134.

Wilks, D.S. (1992) Adapting stochastic weather generation algorithms for climate change studies. *Climatic Change*, **22**, 67-84

Wilks, D.S. (1995) *Statistical Methods in the Atmospheric Sciences*, Academic Press, San Diego, 467 pp.

Woodhouse, C.A. (1997) Winter climate and atmospheric circulation patterns in the Sonoran desert region, USA. *International Journal of Climatology*, **17**, 859-873.

Zebiak, S.E., M.A. Cane and D. Chen (1999) Forecast of Tropical Pacific SST Using a Simple Coupled Ocean-Atmosphere Dynamical Model. *Experimental Long-Lead Forecast Bulletin*, **8**, 1-6.

Zeng, Q.C. (1990) Experiments and Problems of Seasonal and Extra-seasonal Predictions by Using Coupled GCM's. *World Meteorological Organisation, Long-Range Forecasting Research Report No. 13*, 243-248.